frontiers | Frontiers in Earth Science

TYPE Original Research
PUBLISHED 12 November 2024
DOI 10.3389/feart.2024.1472206

OPEN ACCESS

EDITED BY
Jianguo Zhang,
China University of Geosciences, China

REVIEWED BY
Yiquan Ma,
Chengdu University of Technology, China
Rui Zhang,
Peking University, China

*CORRESPONDENCE
Yu Sun,
sunyu_hc@163.com

RECEIVED 29 July 2024
ACCEPTED 29 October 2024
PUBLISHED 12 November 2024

CITATION
Wang X, Sun Y, Yu L, Tang Z, Yan B and Liu R (2024) High-resolution cyclic framework for the Songliao Basin in northeastern China, and its implications for sedimentation and organic matter enrichment.
Front. Earth Sci. 12:1472206.
doi: 10.3389/feart.2024.1472206

High-resolution cyclic framework for the Songliao Basin in northeastern China, and its implications for sedimentation and organic matter enrichment

Xinrui Wang[1], Yu Sun[1]*, Limin Yu[2], Zhenxing Tang[2], Baiquan Yan[3] and Ruhao Liu[4]

[1]School of Earth Science, Northeast Petroleum University, Daqing, Heilongjiang, China, [2]PetroChina Jilin Oilfield Company, Songyuan, Jilin, China, [3]Sanya Offshore Oil and Gas Research Institute, Northeast Petroleum University, Sanya, Hainan, China, [4]Institute of Unconventional Oil and Gas Development, Chongqing University of Science and Technology, Chongqing, China

The study of fine-grained sedimentation has consistently concentrated on investigating the mechanisms and principles governing the enrichment of organic matter. However, the lack of unified stratigraphic framework has always existed as fine-grained sedimentation covers two distinct grain-size grades, namely, mud and silt, which has impeded the progress of subsequent production research. This study exemplified this issue by analyzing the first member of the Qingshankou Formation in the southern Songliao Basin. We established reconstructed gamma and density curves that mitigated filter noise interference, integrated high-resolution sequence results with astronomical cycle divisions, and created a high-frequency isochronous stratigraphic framework for clastic fine-grained sedimentation by leveraging the weak sensitivity of sandstone density curves and the robust stability in eccentricity cycle extraction. This approach addresses the inconsistencies in stratigraphic division methodologies and mismatched outcomes stemming from the use varying techniques to delineate mud and silt components within clastic fine-grained sedimentary sequences. Furthermore, it elucidates how tectonic-scale variations in sediment supply coupled with potential accommodation changes dictate macroscopic stacking patterns within strata, whereas climate fluctuations on orbital time scales govern sand-mud progradation degrees within these layers, culminating in periodic rhythmic characteristics characterized by vertical sand-mud interbedding. A model for stratigraphic development pertaining to lake delta systems constrained by a "synchronous heterotopy" paradigm is proposed for the southern Songliao Basin. The organic matter enrichment pattern aligns with its filling dynamics, indicating an "overfilling" type developmental pattern at lower strata levels where organic material predominantly originates from terrestrial plant debris external to the basin; this material accumulates primarily within silty zones along layers—with areas exhibiting heightened enrichment values slightly lagging behind short-eccentric maxima positions. In contrast, under an upper

"balanced filling" type developmental framework, sources of organic matter are derived both internally and externally relative to the basin—exhibiting substantial heterogeneity—and regions marked by elevated organic matter concentrations are directly associated with locations identified as short-eccentric maxima.

KEYWORDS

astronomical cycle, high-resolution sequence, Qingshankou Formation, Songliao Basin, organic matter enrichment

1 Introduction

The importance of studying fine-grained sedimentary patterns and the accumulation of organic matter (OM) has been highlighted in the exploration of unconventional reservoirs of shale oil and gas. Fine-grained sediments, with particle sizes smaller than 62 μm, are particularly sensitive to minor climatic changes, and exhibit complex lithological, structural, and compositional characteristics that involve a highly heterogeneous OM content (Wang X. R. et al., 2023). The OM within shales significantly influences their potential for hydrocarbon generation as well as the type of reservoir space, reservoir capacity, and the presence of hydrocarbons (Olga et al., 2023; Wang Y. C. et al., 2023; Wang et al., 2022a; Dong et al., 2022; Yu et al., 2020). Therefore, comprehensively understanding the mechanisms and patterns of OM accumulation is crucial for examining fine-grained sedimentary rocks. Two primary hypotheses for OM accumulation are currently in vogue: the model of primary productivity and the preservation model (Calvert and Pedersen, 1993; Tyson, 2005; Bechtel et al., 2012; Jia et al., 2013a). The former emphasizes the influence of OM sources and the strength of primary productivity on OM accumulation, while the latter provides a clearer explanation of the subsequent conditions for OM preservation, such as salinity and redox conditions. Researchers believe that these two models may be jointly applicable to specific sedimentary environments. This suggests that the formation and preservation of OM are complex processes that are influenced by such factors as the terrigenous clastic input and the sedimentary environment (Pan et al., 2021; Song et al., 2016).

Numerous studies have shown that fine-grained lacustrine sediments are more sensitive to changes in the sedimentary environment, paleoclimate, and redox conditions than fine-grained marine sediments. Lacustrine sediments can provide high-resolution records of the terrestrial paleoenvironment. The Songliao Basin in China is a typical basin of the Mesozoic lacustrine revolution (Cohen, 2003), and contains complete and continuous records of the inland environmental climate in the Cretaceous. The Qingshankou and Nenjiang Formations are major source rocks for the Upper Cretaceous in the Songliao Basin, and a considerable amount of research has been devoted to examining their OM characteristics and mechanisms of OM enrichment (Jia et al., 2013a; Jia et al., 2013b). It is widely accepted that marine transgressions during a global rise in sea level (OAE3) led to OM enrichment in the Nenjiang Formation (Liu et al., 2021; Xu et al., 2019; Liu et al., 2022; Cao et al., 2016; Zhang et al., 2020; Zhang et al., 2021). However, debate persists regarding the mechanisms of OM enrichment in the Qingshankou Formation. This is because the southern Songliao Basin is influenced by many factors, including the paleoclimate, lake transgression events, and anoxic events. Many types of fine-grained sedimentary rocks have formed in the first member of the Qingshankou Formation, which has a high heterogeneity (Ma et al., 2022). The terrigenous clastic input near the edge of the lake basin in particular has caused the trend of OM enrichment in the area to be influenced by multiple factors, in contrast to the trend of OM enrichment in the deep-lake area in the northern Songliao Basin. Researchers have used wavelet spectral analysis to identify the astronomical cycles of lacustrine mudstones of the Qingshankou Formation, used this to establish a coupling relationship between the evolution of the sedimentary environment and vertical OM enrichment, and have examined astronomical-scale cycles that drive OM enrichment. Some scholars have analyzed geochemical elements from well GY1, and proposed that a 405 ka long eccentricity controls the cycles of OM enrichment in the Qingshankou Formation (Feng et al., 2023). When the eccentricity is near its maximum, the corresponding sedimentary cycle is in an organic-rich interval. Huang compiled high-resolution datasets of the total organic carbon (TOC) and stable carbon isotope (13Corg) contents of SK1 to investigate its processes of organic carbon burial, and reported a robust cyclicity of TOC of approximately 173,000 years (Huang et al., 2023). The ~173 ka obliquity-related forcing signal was amplified by the internal climatic feedback of the carbon cycle under different geographic and climatic conditions, and led to periodic OM enrichment. However, most such research has focused on vertical variations in the organic matter in single-core wells in the central part of the lake basin, such that a continuous lateral comparison and evolutionary analysis are lacking. A consensus on the periodicity of OM enrichment also remains elusive (Liu et al., 2022; Wang X. R. et al., 2023; Xu et al., 2015; Zhang et al., 2022; Liu et al., 2021; Wang M. et al., 2023; Liu et al., 2021; Wang H. R. et al., 2023).

The area of hydrocarbon exploration in the first member of the Qingshankou Formation (referred to hereinafter as the "First Member") in the southern Songliao Basin is located at the terminus of a deltaic depositional system. When analyzing the mechanisms of OM enrichment, it is important to integrate the near-source terrigenous clastic influences within a shallow lake with the sand-rich environment. A unified model of this is lacking because researchers have investigated OM contents in different locations without using a common temporal framework. A coherent, high-frequency, sequential stratigraphic framework that can cover the area from the sand-rich lake margin to the mud-rich center of the lake is needed to this end.

The conventional clastic strata along the margin of the basin and the mudstone strata at the center of the lake are often discussed

separately in currently used high-frequency sequential stratigraphic divisions of the Qingshankou Formation in the southern Songliao Basin. Traditional and high-resolution sequential stratigraphy are still used for dividing clastic strata, while cyclic stratigraphy is applied to mudstone layers at the center of the lake by using astronomical rhythms (Wu et al., 2009), and T-R (Cheng et al., 2003) and GPR sequences (Du et al., 2016) are used to restore the characteristics of depositional rhythm of mudstone to construct its spatio-temporal order. Both high-resolution sequences and astronomical Milankovitch cycles play a vital role in establishing the framework for fine-grained lacustrine sedimentary strata. Despite their interconnections, however, differences in their foci of research, scales, and emphases prevent a clear correlation between them.

High-resolution sequential stratigraphy is significantly influenced by subjective human decisions (Cross, 1994), and identifying the data surfaces in mud-rich areas is challenging. Although astronomical cycles offer a higher resolution, they are suitable only for analyzing continuously deposited and tectonically stable mudstone strata. Astronomical noise, such as that owing to autocyclic processes, obscures the clear identification of the cycles in sand-rich areas. Thus, the high-resolution sequential stratigraphic results for the margins of terrestrial lakes and mud-rich lake centers cannot be integrated, and this leads to a "segmented, blocky, and methodological" characteristic in a basin-wide sequential framework of analysis (Sun et al., 2017; Wu et al., 2009; Zhang et al., 2019).

Both astronomical cycles and high-resolution sequential stratigraphy fundamentally describe the repetitiveness of the strata, and represent branches of cyclostratigraphy at different scales (Zheng et al., 2001; Wang et al., 2018). In light of this, we use the floating astronomical timescale of the Songliao Basin as a reference to combine these cyclostratigraphic methods based on Milankovitch's theory such that this yields the advantages of high-resolution sequential stratigraphy. We then compare the characteristics of sequential development of deep-water mud-rich zones and shallow-water sand-rich zones within fine-grained sedimentary systems. Following this, we construct the corresponding relationship between astronomical cycles (long eccentricity, short eccentricity, obliquity, and precession cycles) in the mud-rich center of the lake basin and the base-level cyclic hierarchies (fourth to seventh order) in the shallow-water sand-rich margins.

This study bridges the gap between the results of high-resolution sequential stratigraphy of the margins of the lake basin, and those of the division of the astronomical cycles of the lake center to establish a high-frequency sequential stratigraphic framework that is constrained by astronomical cycles. This framework restores the ordered spatio-temporal relationships of the complex strata, and can be used to identify the pattern of evolution of the depositional sequence along the margins of continental rift lake basins. Based on this, we use the tectonic and orbital timescales in conjunction with the differences in OM characteristics to extract the important factors controlling OM enrichment. We also establish a model of OM enrichment in fine-grained sediments under strong terrigenous clastic influences.

2 Geological setting

2.1 Tectonics and sedimentation

The Songliao Basin is a large-scale Mesozoic–Cenozoic petroleum-bearing continental sedimentary basin in northeastern China, with a dual structural feature of an initial fault-induced depression followed by a superimposed depression in the NNE direction (Feng et al., 2010). The foundation of the basin consists of Carboniferous–Permian metamorphic rocks and granite, while the sedimentary cover includes Jurassic, Cretaceous, Paleogene, Neogene, and Quaternary deposits (Figure 1C). Based on the properties of the basement rocks and the regional geological characteristics of the caprock, the structural layers of the depression in the Songliao Basin can be divided into six first-order structural units, which are believed to control the distribution of reservoirs for oil, natural gas, shale gas, and oil sands (Figures 1A, C). The central depression has long been the sedimentary and subsidence-related center of the Songliao Basin, and almost all of its strata are well developed. The thickness of the Cretaceous stratum exceeds 6500 m, and it contains two kinds of high-quality rocks that are the source of hydrocarbons: First Member and the Second Member of the Nenjiang Formation (Liu et al., 2019).

The Songliao Lake Basin underwent significant subsidence and expansion, and developed a water inlet system during the development of the Qingshankou Formation, especially in the early stages of formation of the Qingshankou section when the rate of expansion of the water surface was the highest. Analyses of the stratigraphy and the thickness of the mudstone layer show that the depositional center of the depression extends along Qijia, Gulong, Daan, Changling to Lishu, and Sanshao to Dewei (Sun, 2010). The rate of subsidence of the sedimentary system in the lake basin extension is greater than the rate of sedimentation, and has led to a landward retreat of the background (Wang et al., 2007; Wang et al., 2009) such that only the Tongyu–Baokang sedimentary system remains intact. Its depositional end is the shale area of the southern Songliao Basin (Wang M. et al., 2023; Li et al., 2020). Unlike the shale oil-rich Qijia–Gulong Sag in the north of the Songliao Basin, where dark mudstone and shale that are rich in organic matter are deposited in deep and semi-deep lake facies, the organic-rich shale in the south is located in the outer front surfaces of the delta (shallow lake facies) of the Daqingzijing area, which is more severely affected by terrigenous debris (Figure 1B).

2.2 Sequential stratigraphy

The Cretaceous system, featuring a continental clastic rock mixed with a sedimentary formation of oil shale (Figure 2A), was the main sedimentary stratum during the depression of the Songliao Basin. It can be divided into upper and lower series, consisting of nine formations and 27 lithological sections. The period considered here pertained to the First Member of the Upper Cretaceous (hereinafter referred to as Qn1). This period featured a rapid expansion of the lake basin during the early stage of the overall depression of the Songliao Basin. The basin

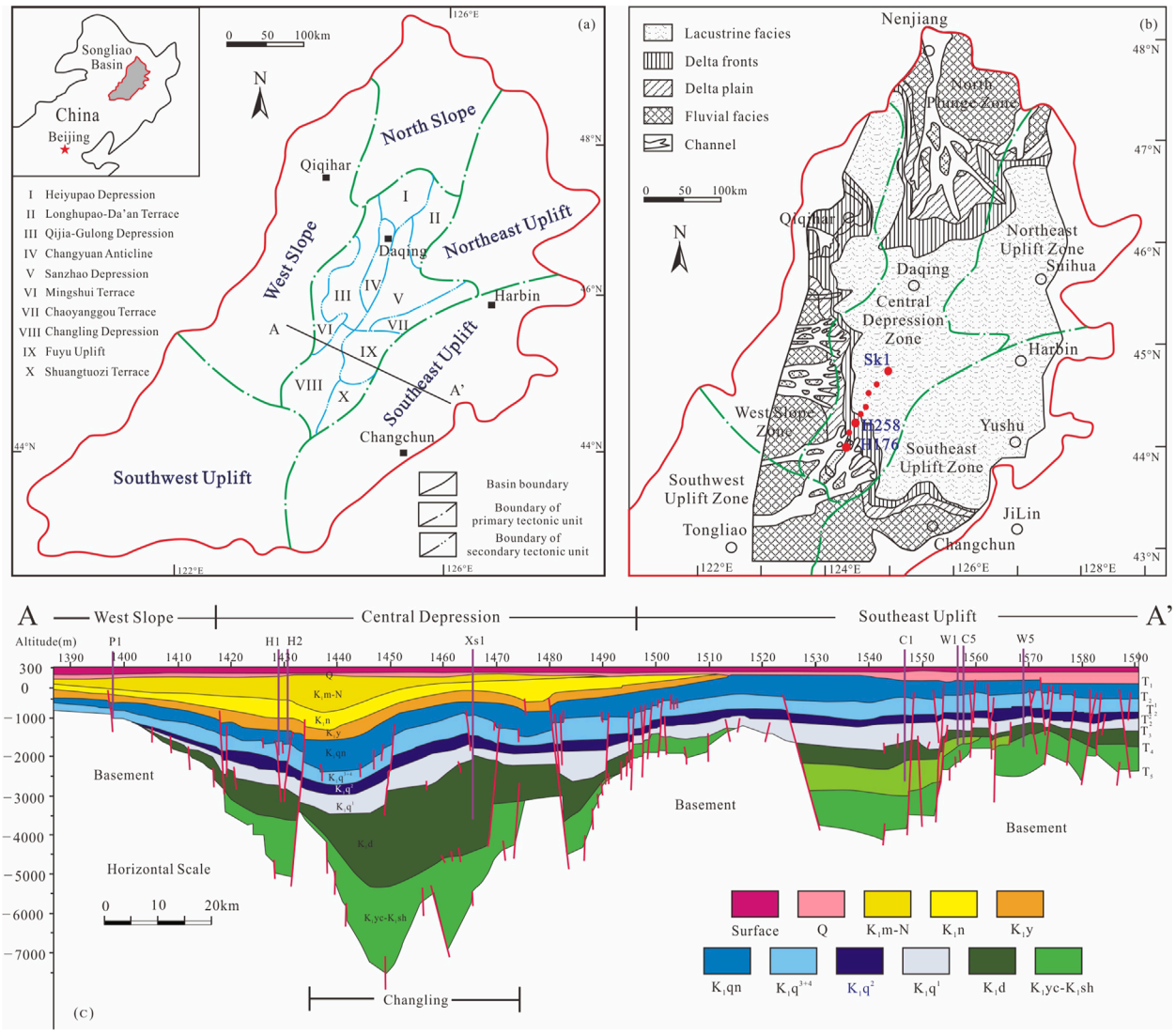

FIGURE 1
Tectonic position and comprehensive stratigraphic map of the study area in the southern part of the Songliao Basin (Liu et al., 2023; Wu et al., 2009). **(A)** Location map of the Sanzhao depression and tectonic units of the Songliao Basin. The black line (AA') shows the location of the stratigraphic profile (Figure 1C) of the Songliao Basin. **(B)** The locations of the study area and important wells considered in this study. **(C)** Stratigraphic section across the central part of the Songliao Basin, showing its structure.

was dominated by delta and lake sedimentary systems, and its lithology involved greyish-green, dark mudstone, and a dark-gray siltstone interbedding, while the bottom often featured dark mudstone.

Wu et al. have continually sought to calibrate the astronomical age of the Qingshankou Formation in the Songliao Basin since 2009 (Wu et al., 2009). They used information acquired from well SK1 to determine the presence of an astronomically driven Milankovitch sequence within the Qingshankou Formation. They also established the floating astronomical scale (ATS) by combining radioisotope ages and paleomagnetic analyses (Figure 2B). They concluded that the three sets of oil shale and black shale deposits at the bottom of the First Member in the Songliao Basin can be attributed to the first anoxic event of the lake basin (LAE1). This event corresponded to the Late Cretaceous Cenomanian–Late Turonian–Early Oceanic anoxic event (OAE2) (Demaison and Moore, 1980), which constrained the timeframe of development of the Qingshankou Formation such that its absolute geological age was determined to be 91.341 Ma. It was located in the lower 20 m of LAE1—at the junction of the sandstone and mudstone between the fourth and first members of the Qingshankou Formation, and the underlying Quantou Formation (Wu et al., 2009; Wu et al., 2013; Wu et al., 2014; Wu et al., 2022).

However, when analyzing sedimentary and tectonic evolution as well as oil shales, the First Member in the Songliao Basin is usually considered to be the boundary between the Quantou Formation and the Qingshankou Formation, with the oil shale at the bottom of the First Member designated as the boundary between them (Liu et al., 2019). Owing to the large deposition

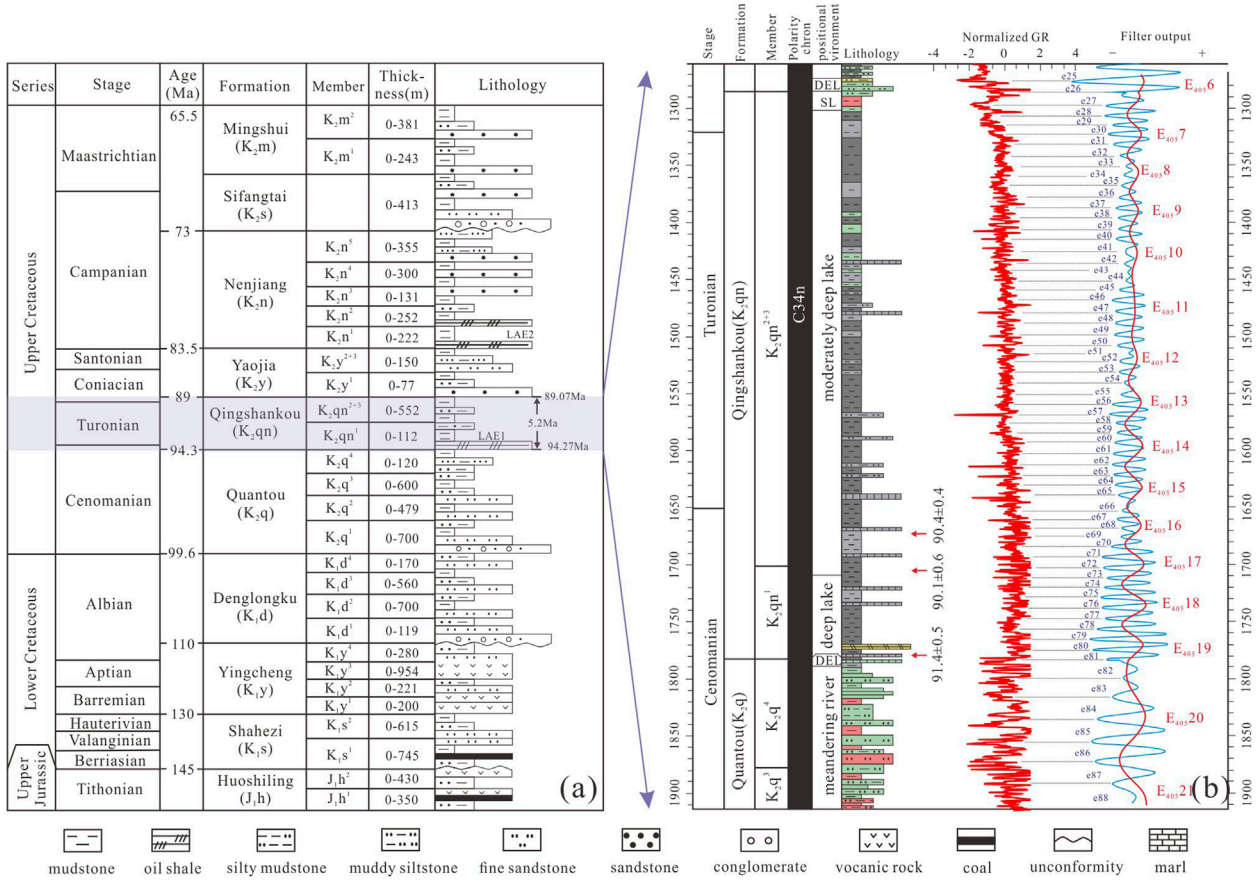

FIGURE 2
Extent of the target layer, and characteristics of the lithology and the astronomical cycle (Modified by Wu et al., 2009; Wu et al., 2013). **(A)** Comprehensive stratigraphic characteristics of the Cretaceous system in the Songliao Basin. **(B)** Compilation of key data showing the stratigraphy, polarity chron, paleoenvironments, lithology, SIMS U–Pb zircon ages, and cyclostratigraphic interpretation of the SK-Is borehole in the SLB. "e" (blue) and "E" (red) represent 100 ka short and 405 ka long eccentricity cycles, respectively. The interpreted 100 ka and 405 ka eccentricity cycles were extracted by using Gaussian bandpass filters. Filter passband for 405 ka eccentricity cycles: K_2qn—0.0261 ± 0.005 cycles/m. Filter passband for 100 ka eccentricity cycles: K_2qn—0.113 ± 0.025 cycles/m.

in sand-rich areas along the edge of the basin, it is difficult to distinguish between the bottom of the Qingshankou Formation and the sandstone of the underlying Quantou Formation (Xu et al., 2019b). For the sake of convenience, we follow past research and set this boundary at the bottom of the First Member, i.e., the bottom of the first set of oil shales corresponding to the bottom of event 2023 of LAE1 (OAE2). This boundary is useful for the subsequent analysis of sedimentation and patterns of OM enrichment.

3 Methods and dataset

3.1 Data selection

Starting from well SK1 in the deep lake region of the Qingshankou Formation in the southern Songliao Basin, our research extended southward toward the delta front of the Daqingzijing area, passing through areas with wells such as Xinbei, Miaoxi, and Qian'an. The total number of wells exceeded 4,000, including conventional logging sequences such as GR, AC, DEN, and R, and unconventional logging sequences like imaging logs and elemental logs. Based on the characteristics of stratigraphic development, we chose wells near the lake area (SK1, NEN8, XIN342, XIN328, RANG32, QIAN189) and those in the deltaic sedimentary region along the margin of the lake basin (QIANSHENG11, HEI258, HEI197, CHANGSHEN107) to analyze the astronomical cycle (as shown in Figure 1). We plotted complete curves of the natural gamma ray (GR), spontaneous potential (AC), density (DEN), and resistivity (R) of all wells in the Qingshankou Formation. We also considered seven cored wells and analyzed over 120 core samples to examine their lithological and mineral compositions as well as their OM characteristics. Wells SK1 and HEI258, which were located in the deep-lake mud-rich area and the sand-rich area along the margin of the lake basin, respectively, were highly comparable and have been well documented. These were thus important for the analysis of the astronomical cycle provided in this study.

3.2 Sequential stratigraphic analysis

Variations in Earth's orbital parameters cause changes in the amount of solar radiation received per unit area by its surface. These changes in the solar radiation can alter patterns of atmospheric circulation, causing latitudinal shifts in climate zones, and resulting in changes in the atmospheric temperature, ocean circulation, and precipitation. Changes in climate in turn influence glacial activity, the flow of rivers, and the strength of wind to further impact the processes of weathering, transport, and deposition. Changes in solar radiation also influence the influx of nutrients into lakes, evaporation from them, and processes of marine and lacustrine circulation. All these interrelated factors ultimately control the formation of sedimentary products, which are expressed in strata as rhythmic or cyclic variations in the lithology, facies, or geochemical parameters to form stratigraphic cycles that are consistent with astronomical orbital cycles.

Elements of the Milankovitch cycle can be used to establish high-frequency sequential stratigraphic frameworks for fine-grained sediments (Milankovitch, 1941). Astronomical cycles based on Milankovitch's theory include cycles with long eccentricity, short eccentricity, obliquity, and precession. By establishing a correspondence between the astronomical cycles and base-level cycles, the temporal properties of the former can be used to constrain the latter, such that this can reduce the influence of subjectivity and human bias on the division of base-level cycles.

Compared with previously reported extractions of astronomical cycles in the context of fine-grained sediments, the lacustrine sediments of the First Member encounter challenges in terms of astronomical tuning owing to frequent terrigenous clastic inputs. Regions with deep lakes exhibit clear boundaries of the astronomical cycle, such as well SK1 (Wu et al., 2013). However, closer proximity to the source of the sediment in shallow lakes and outer front areas increases noise during astronomical tuning. Conventional methods of data preprocessing, such as detrending, fail to eliminate this noise, and it requires techniques for the targeted reconstruction of the curves of astronomical tuning.

3.3 Methods of time series analysis

We conducted experiments on cyclic analysis by using Acycle V2.4.1 in the MATLAB platform.

3.3.1 Data selection

Before conducting cyclostratigraphic analysis, we needed to choose suitable proxy indicators for the paleoclimate. The gamma ray (GR) curve preserves the primary signals related to climate change, Moreover, the paleoclimate reflected by the GR curve is not influenced by such factors as sedimentary hiatus and diagenesis (Kemp, 2011; Hilgen et al., 2015). High GR values indicate warm and humid conditions owing to the greater input of clay minerals, and organic matter from enhanced chemical weathering and precipitation. Conversely, low GR values indicate cold and dry conditions owing to greater physical weathering and reduced vegetation, which lead to a decreased input of clay and an increased input of inorganic carbonates. Traditional studies have primarily used the GR curve to examine the astronomical cycle (Li et al., 2019; Boulila et al., 2021; Li et al., 2016; Xu et al., 2019a; Li et al., 2018). However, frequent interactions with the terrigenous clastic input increases noise in the astronomical tuning of continental depositional environments, and conventional methods of data preprocessing like detrending cannot eliminate this noise. To accurately extract astronomical cycles from data on fine-grained sediments in areas with shallow lakes, the obtained curves need to be reprocessed to weaken the noise from terrigenous inputs. Researchers have used the curves of density to extract astronomical cycles in past work. We combined the curves of density, which have a low sensitivity to radioactivity, and weak responses to sand and mud, with the GR curve to analyze the astronomical cycle in shallow-lake areas.

3.3.2 Curve fusion

We subjected logging data from the shallow-lake region of K_2qn^1 to a sensitivity analysis. The GR curve is sensitive to lithological changes, and thus can be used to clearly identify lithological variations like thin layers of sand (Hesselbo, 1996). By contrast, the DEN (density) curve has a wide zone of transition that can be used to identify sand and mud. An analysis of the correlation between these curves shows that the GR curve has a larger difference in amplitude between lithologies, particularly between sandstone and mudstone, while the DEN curve has a larger difference in amplitude for mudstone and a smaller difference for sandstone. Therefore, noise from the auto-cycles can be weakened by reconstructing the GR curve based on trends of the curve of density such that it features the strengths of both kinds of curves. This method retains the stability of the curve of density in reflecting sand–mud transitions, while preserving the detailed characteristics of the GR curve for sections of mudstone. The main steps are as follows: 1) Normalize the curves of sand and mud. 2) Determine the threshold of sandstone-related anomalies in the GR curve and calculate its index. 3) Separate high and low frequencies in the curve of density to obtain the differences in high- and low-frequency amplitudes. 4) Calibrate the amplitude of the curve of the anomaly index by using the differences in high- and low-frequency amplitudes of the curve of density. 5) Reconstruct the characteristic GR curve Equations 1–3:

$$GRS = ((GR\text{-}GRmin(sand)/(GRmax(mud)\text{-}GRmin(sand))/G \quad (1)$$

$$DENS = ((GRS\text{-}GRSmin)/(GRSmax\text{-}GRSmin) + 1) * C \quad (2)$$

$$GRR = DENF + B + DENS \quad (3)$$

where GRS is the anomaly index, GR represents natural gamma rays, GRmin(sand) and GRmax(mud) are the natural gamma ray values for stable sandstone and mudstone, respectively, G is the threshold of the anomaly for sandstone, DENS is the amplitude-normalized anomaly index of the density, GRSmax and GRSmin are the maximum and minimum values of the index of anomaly in sandstone, respectively, C is the original difference in the high-/low-frequency amplitudes of density, GRR is the reconstructed curve, DENF is the low-frequency curve of density, and B is an empirical coefficient (ranging from zero to one). Its value is chosen to ensure that the reconstructed GR reflects the original trend, and it uses the curve of density to weaken anomalies close to the values for

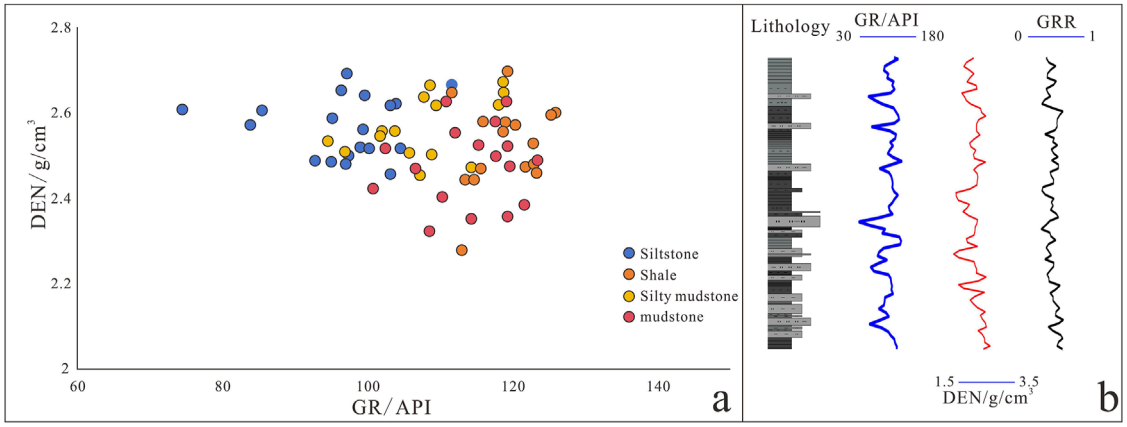

FIGURE 3
Reconstruction of the GR and DEN curves. **(A)** The GR curve is highly precise in identifying sandy bodies with different lithologies, with a numerical range greater than that of the DEN curve. The DEN curve is less sensitive to lithological changes than the GR curve. **(B)** The reconstructed GRR curve retains the characteristics of the original GR curve while using features of the DEN curve to reduce variations in the amplitude caused by frequent sand–mud interbedding.

stable sandstone. The reconstructed GRR curve weakens anomalies in the GR brought about by the development of sand bodies in the foreground (Figure 3).

3.3.3 Data preprocessing

Raw data contain environmental noise that can affect the accuracy of the subsequent experimental results. Therefore, we preprocessed the data before analyzing the cycles:

1) We used the "Sort/Unique/Delete-empty" package to remove outliers that deviated from the normal range of fluctuations, duplicates at the same depth, and empty values.
2) We used the "Interpolation" package to perform linear interpolation and ensure that the data were equidistant.
3) We used the "Detrending" package by using the LOWESS method to eliminate the long-term suppression of high-frequency signals.

3.3.4 Cycle analysis

Spectral Analysis: We applied the multi-taper method along with the robust AR red noise model confidence test to extract significant peaks with a confidence level of >90%. The graph of the spectrum showed the distribution of signal power within the spectral range, with the *x*-axis representing the frequency (its inverse represented the corresponding cycle thickness) and the *y*-axis representing the relative amplitude of the target frequency.

Sliding-window Spectral Analysis: We used the fast Fourier transform (FFT) to obtain the spectra of evolution in the depth domain. This provided a visual representation of changes in the rate of sedimentation along the vertical axis while identifying potential interruptions in sedimentation.

Filtering: We extracted specific mixed and overlapping stratigraphic signals by using the filtering operation. We applied the high-pass operation of the Gaussian filter to set the center frequency and filter bandwidth, and used them to extract potential signals of the target orbital.

3.3.5 Wavelet analysis

The continuous wavelet transform is used for wavelet analysis. Wavelengths with a high power and relative continuity in the spectrum are the main features of the continuous wavelet transform. Wavelet analysis is a time–frequency method of analysis that can localize the signal in the time and frequency domains. It can extract local features of the signal, including changes in its frequency and energy. We used wavelet analysis to identify the dominant cycles in the formation.

3.3.6 Modeling sedimentary noise

Sedimentary noise can be modeled to analyze the dynamics of the signal-to-noise ratio in proxy data on the climate (Li et al., 2018). It is a powerful tool for reconstructing the levels of both seas and lakes in marginal marine and lacustrine paleoenvironments. The DYNOT model is designed to measure noise in data on the climate and proxies of water depth (Wang et al., 2020), such as those in the GR signals in this study. It is based on establishing the ratio of variance in the signal that is unrelated to orbital forcing (i.e., noise) to the total variance in the dataset. All modeled sedimentary noise presented here was computed by using DYNOT functions in Acycle v2.4.1 (Li et al., 2019). All the periodograms, and the steps of the AM and F-test were also executed by using Acycle v2.4.1.

4 Results

4.1 Sequential stratigraphic analysis

4.1.1 Tectonic timescale: high-resolution sequential stratigraphic framework

Sedimentary systems are primarily driven at the tectonic timescale (usually greater than 1 Ma) by interactions among the Earth's spheres (Houston, 2004; Cross, 1194). The balance between the climate-driven supply of sediment and the space

to accommodate it at this scale, which is controlled by tectonic subsidence and lake-level fluctuations, is the key factor influencing the characteristics of the sequence as well as the types of internal sediments, their patterns of distribution, and evolutionary characteristics (Carroll and Bohacs, 1999). High-resolution sequential stratigraphy is commonly used to analyze sedimentary systems at this scale.

In light of past research (Wang, 2022b), we used the high-resolution sequential stratigraphy of the sand-rich area on the margin of the lake basin to divide the strata into one long-term base-level cycle (LSC1), four mid-term cycles (MSC1–MSC4 from bottom to top), and 16 short-term cycles (SSC1–SSC16 from bottom to top). The short-term base-level cycles were of four types: asymmetric up-deepening cycle (A), asymmetric "up-shallowing" cycle (B), symmetric cycle (C1), and incomplete symmetric cycle (C2). The positions of spatial development, types of internal sediments, and characteristics of different cycles varied.

We obtained several insights by analyzing the patterns of vertical variations in the ratio of the space to accommodate the sediment (A) to its supply (S), based on the characteristics of internal development of sand bodies within distinct cyclic structural patterns (Figure 4). The mid-term base-level cycles in the First Member exhibited a pronounced dichotomy. During the MSC1–2 depositional periods in the lower section, the long-term base level rose steadily and gradually, and manifested as the vertical periodic superposition of multiple short-term cycles of types A, C1, and C2. At this time, the transition from $A/S < 1$ to $A/S > 1$ suggests that the rate of sediment supply at the base—near the main flowline—exceeded the potential rate of growth of the space to accommodate it, and led to the superimposition of sand bodies that was represented by sparse type-A features. As the lake level rose, the space for accommodation expanded, and the supply of sediment became insufficient to fill this space. Consequently, the capability of incision of the river weakened while lateral erosion intensified, leading to a transition in the process of deposition from progradation to aggradation. The sedimentary record of the rising hemicycle within this type of mid-term base-level cycle remained intact. The base was characterized by weak erosion, or abrupt lithological transitions between sandstone and mudstone, with internal muddy and silty laminae common between them. Conversely, the upper MSC3–4 section was dominated by descending hemicycles, corresponding to the decline of the long-term base level, and comprised short-term base-level cycles of types B and C2. Cycles of types B, C2, and A were observed along the margins of the lake basin and near the main flowline. As the space for accommodation consistently exceeded the flux in the supply of the sediment ($A/S > 1$) in this period, a state of under-compensated to weakly compensated deposition emerged to form vertically composite, inversely rhythmic sedimentary sequences that were characterized by aggradational–retrogradational patterns.

4.1.2 Orbital timescale: stratigraphic framework of astronomical cycle

We used the standard modeling scheme developed by Laskar et al. to extract the theoretical cyclic curves of eccentricity and cyclic variations in the slope during 85–95 Ma in the Cretaceous, as a benchmark for determining the astronomical cycle (Laskar et al., 2011). We analyzed the spectra of multiple wells, with SK1 as the starting point, along the direction from the center of the lake basin toward the shallow-water area. We considered the horizontal coordinates of the multi-frequency spectrogram as the cyclotomic frequency of the depth sequence, obtained the frequency of the dominant cyclotomic cycle with a confidence of higher than 95%, and compared it with the theoretical orbital period. The frequencies were 0.0206 cycle/m, 0.0887 cycle/m, and 0.211 cycle/m. The ratio of the inverse was 10.41:2.37:1, which is very close to the ratio of 10.8:2.67:1 at 405 ka (long eccentricity), 100 ka (short eccentricity), and 37.5 ka (slope) for the Earth's orbital parameters. We analyzed six typical wells in the near-deepwater area (SK1, N8, X342, X328, R32, and Q189), and found that all of them followed the sequence of Miskovic rotation (Table 1; Figure 5).

A set of high-confidence frequencies, with an average of about 0.02341 cycles/m, and a cycle thickness of 41.4 m were identified in the astronomical cycle based on the GR curve, and conformed to the characteristics of the 405 ka long eccentricity cycle. Moreover, the characteristics of variations in the curve corresponding to the maxima and minima of this cycle were consistent with those of well SK1 in the deep-lake area. This indicates that the long eccentricity with a longer cycle persisted in the shallow-lake area, and controlled the long cyclic interface of the First Member in the deep-lake and outer front areas. The confidence of each cycle within the range of the short eccentricity cycle was complex. There were two distinct high-confidence cycles of 90.1 ka and 81.1 ka that deviated significantly from the short eccentricity cycle in the deep-lake area. If the short eccentricity was extracted according to different ranges of depth, the number of extracted short eccentricities in the upper long eccentricity center E2 was not significantly different from that in the deep-lake area, while the number of short eccentricity cycles in the lower long eccentricity E1 significantly increased. The reconstructed curve of GRR was able to more accurately extract the astronomical cycles in the shallow-lake area, which is consistent with the results for well SK1 in the deep-lake area (Figure 6).

The astronomical cycles extracted based on the GR curve, from well SK1 in the deep-lake area to the edge of the lake basin, showed approximately 1.8 cycles of the 405 ka long eccentricity, seven cycles of the 100 ka short eccentricity, and 21 cycles of 37.5 ka obliquity. These cycles could still be identified in well R30 along the edge of the basin, and matched those of well SK1 (Figure 7). The consistency of the astronomical cycles weakened from south to north toward the edge of the lake basin. Owing to filtered noise from terrigenous clastic inputs, the GRR curves derived from the fusion of the GR and DEN curves were used to extract the astronomical cycles in the marginal front area. This method was also used to successfully identify stable cycles of 1.8 for the 405 ka long eccentricity and seven for the 100 ka short eccentricity. Therefore, stable eccentricity cycles could be extracted by using both the basic GR curve and the reconstructed GRR curve.

4.1.3 Integration of sequential stratigraphic frameworks

To integrate astronomical cyclic stratigraphy with high-resolution sequential stratigraphy, a matching relationship needed to be established between these frameworks. The accuracy of extraction of the astronomical cycles gradually decreased from

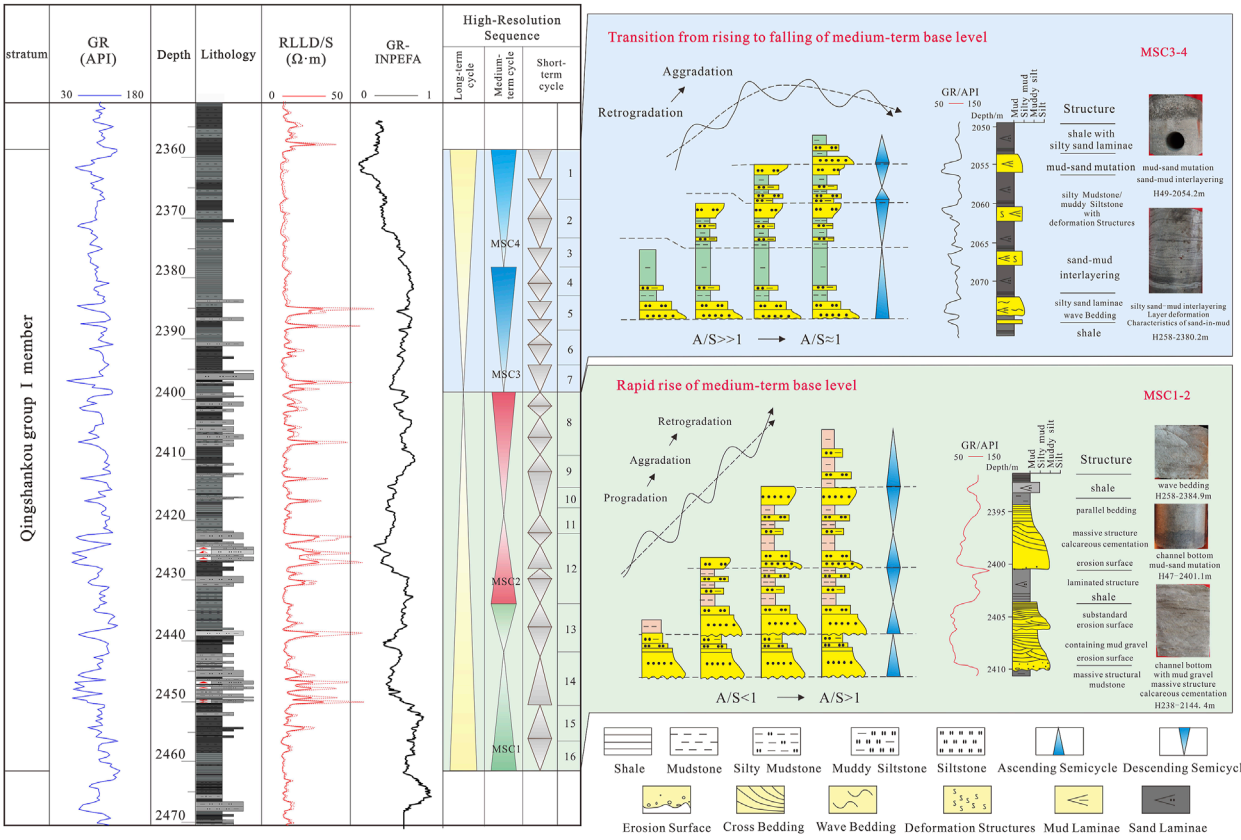

FIGURE 4
Scheme of mid-term base-level cycles in K_2qn^1 and their patterns of stratigraphic stacking, with the depositional characteristics obtained from well Hei 258. The long-term base level in the study area exhibited a complete transgressive–regressive cycle with a distinct bipartite nature. The long-term base level in the lower part rose steadily, and the rate of sediment supply exceeded the rate of growth of the potential accommodation for it, resulting in retrogradational and aggradational stacking patterns. The cycles were primarily asymmetric, and were dominated by either rising or falling phases that constituted the mid-term and short-term base-level cycles of this period, respectively. The upper part corresponded to the transition from rising to falling long-term base level. During this time, the space for accommodation was large but the supply of the sediment was insufficient to fill it, resulting in underfilled to weakly compensated depositional conditions. This led to the formation of multiple, vertically compounded mid-term and short-term base-level cycles with aggradational–retrogradational stacking patterns in an anti-thetic manner.

well SK1 toward the shallow lake. Astronomical cycles could be extracted from sandy areas in the shallow lake by sacrificing the precision of vertical resolution of the GR curve and reducing noise arising due to the development of the sand body. The high-resolution sequences were distinguishable at the edge of the lake basin, but it became challenging to identify them at the center of the basin, which featured reduced development of sand. We integrated the two methods by using data on wells close to the zones of overlapping confidence as bridges. This process involved assigning temporal significance to the high-resolution sequential stratigraphic framework and structural characteristics to the framework of astronomical cycles.

A comparison of the high-resolution sequences in sandy areas with the stratigraphy of the astronomical cycles in muddy areas revealed some correspondence as well as differences between them. We identified three long eccentricity maxima of 405 ka in the first section, with four long eccentricity cycles between them. These cycles were controlled by the climate and tectonics, and represented secondary lake transgression–regression cycles that reflected changes in the climate, temperature, and intensity of terrigenous clastic input.

We identified eight maxima of 100 ka short eccentricity and 14 cycles in the first section, where this was correlated with the sediment facies and trends of mineral composition. Moreover, we identified 22 maxima of 37.5 ka obliquity cycles that formed 42 obliquity cycles. The mid-term cycles in the high-resolution sequences corresponded well with the long eccentricity cycles, while the short-term cycles differed due to over-differentiation between sand and mud in the high-resolution sequential division. This led to the breakdown of the symmetrical cycles into asymmetrical ones. We established a more comprehensive process of lake transgression–regression by constraining the lower sandy zone with the astronomical cycles. Our observations showed that neither the failure of high-resolution sequence stratigraphy owing to unrecognizable base-level characteristics in mudstone, nor the failure of the astronomical cycles owing to sedimentary noise caused by spin-back was sudden. There was a superimposed zone of confidence between them. The integration of the results of these

TABLE 1 Frequency of deep-cycle sequences *versus* the astronomical cycles of orbits.

Well ID	Frequency/(cycle/m)	Cycle thickness/m	Ratio	Periodic ratio of theoretical orbit	Period of theoretical orbital/ka
SK1	0.02026	49.3583	10.41	10.8	405
	0.0887	11.2739	2.37	2.67	100
	0.211	4.7393	1	1	37.5
Nen8	0.0221	45.2488	10.97	10.8	405
	0.101	9.9009	2.40	2.67	100
	0.2425	4.1237	1	1	37.5
Xin342	0.0245	40.8163	10.30	10.8	405
	0.098	10.2040	2.57	2.67	100
	0.2525	3.9603	1	1	37.5
Xin328	0.0267	37.4531	10.63	10.8	405
	0.12	8.33333	2.36	2.67	100
	0.284	3.52112	1	1	37.5
Rang32	0.0189	52.9100	10.845	10.8	405
	0.081	12.3456	2.53	2.67	100
	0.205	4.8780	1	1	37.5
Qian189	0.0224	44.6428	10.40	10.8	405
	0.0954	10.4821	2.44	2.67	100
	0.233	4.29184	1	1	37.5

two sets of stratigraphic divisions in the confidence zone solved the problem of constructing the stratigraphic framework of clastic fine-grained sedimentary rocks that are significantly influenced by land-borne debris (Figure 8).

4.2 Characteristics of tectonic and orbital timescales

The fundamental concept of continental sequential stratigraphy is that the geometry and lithology of the stratigraphic units are controlled by four major factors: tectonic subsidence (which dictates the space to accommodate sediment deposition), lake-level changes (which control the stratigraphy and patterns of the facies), paleoclimate (which influences the types of sediment), and sediment supply (which governs sediment fill and paleodepth). Moreover, sudden marine transgressions and volcanic activities may impact these units. Climatic conditions mainly influence the types of sediment, while tectonic subsidence and sediment supply collectively control the internal composition and morphology of the sequences.

4.2.1 Analysis of environmental evolution at tectonic timescales

4.2.1.1 Characteristics of restoration of accommodation space for sediment (parameter A)

The characteristics of the space to accommodate the sediment were primarily influenced by the paleotopography and paleodepth, with a minor change in the overall paleoslope (0.013°). The space for accommodation (A) was mainly controlled by lake-level fluctuations while the rate of sedimentation reflected the supply of the sediment (S). The characteristics of environmental evolution at the orbital timescale indicate that the paleoclimate became increasingly humid during the K_2qn^1, leading to deeper lakes. The results of the DYNOT model showed that the lake levels were relatively low during MSC1–2, began to rise after MSC3, and peaked during MSC4. Therefore, changes in the space for accommodation (A) around the Daqingzi well during K_2qn^1 were mainly related to changes in the depth of the lake (Figure 9).

4.2.1.2 Restoration of sediment supply (parameter S)

The supply of sediment was jointly controlled by the depositional environment, temperature, and climate. The characteristics of

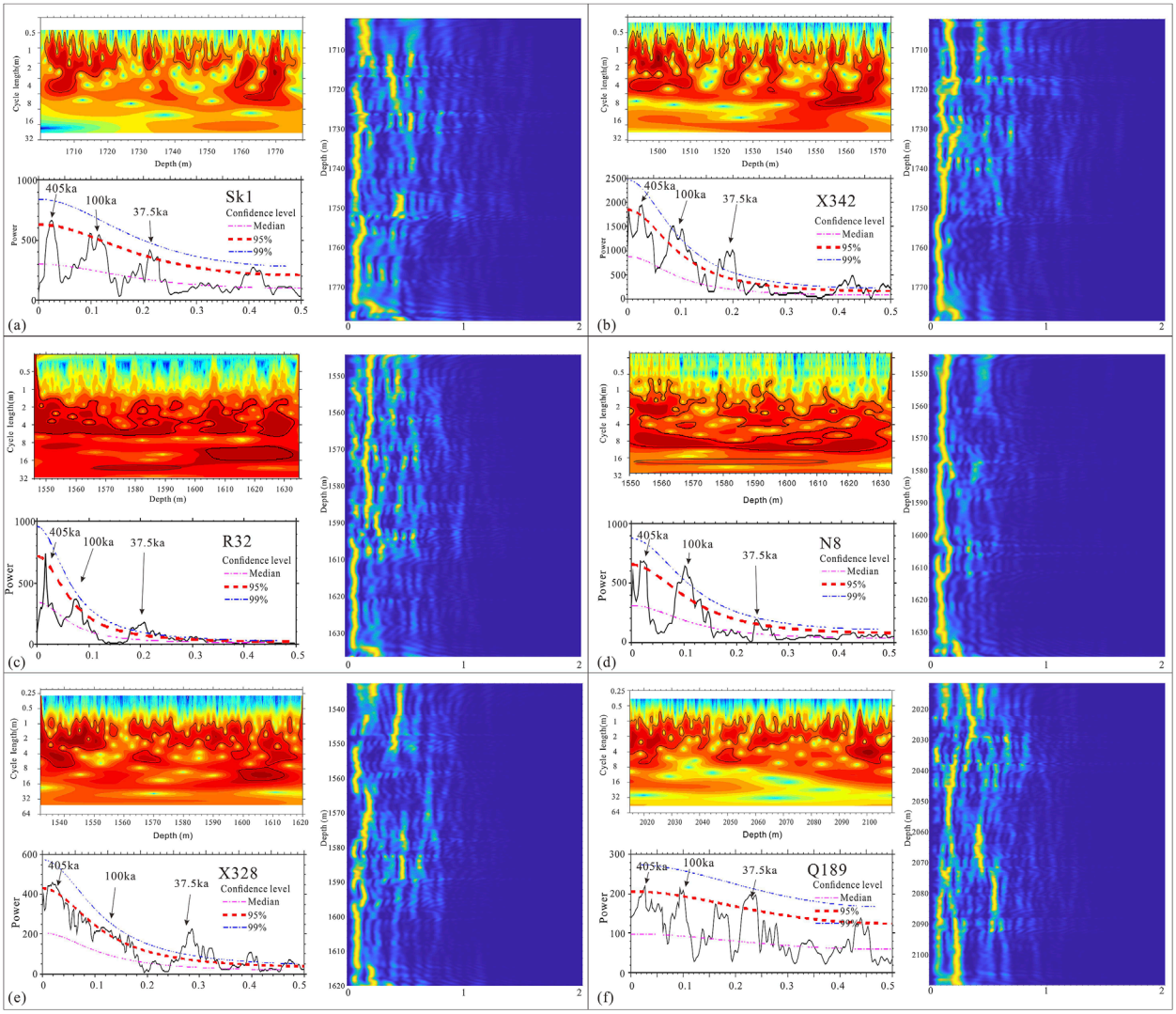

FIGURE 5
The 2π MTM (multi-taper method) power spectra, wavelet scalograms, and evolutionary spectrum of GR logging data from the First Member. Data on six wells in the mud-rich area are shown as examples (SK1, R32, X328, X342, N8, Q189). We show the spectra of the wavelet power and frequency of each well. The purple curve "Median" represents the smoothed and fitted red-noise spectrum. The blue and red curves represent 99% and 95% confidence levels, respectively. The shaded contours in the wavelet scalograms are normalized linear variances, with blue representing low spectral power and red representing high spectral power.

environmental evolution at the orbital timescale revealed that the depositional environment, as reflected by tests of the elemental and grain sizes (Figure 10), was generally reductive during K_2qn^1, with increasing reductiveness and humidity from bottom to top. The rate of sedimentation reflected the sediment supply (S), was high during MSC1 and MSC2, and gradually decreased upward.

In summary, the K_2qn^1 exhibited a dichotomy at the tectonic timescale: There was a gradual increase in the space for the sediment and a gradual decrease in the rate of sedimentation from bottom to top, with frequent internal fluctuations. The lower MSC1 and MSC2 periods featured higher sedimentation rates and smaller spaces to accommodate the sediment, thus exhibiting the characteristics of transitional filling, while the upper MSC3 and MSC4 periods had the opposite trend, with characteristics of balanced filling.

4.2.2 Analysis of environmental evolution on orbital timescale

High-frequency fluctuations in the depths of lakes on an orbital timescale are largely controlled by the climate. The configuration of the Earth's orbital parameters influences the distribution and intensity of the solar radiation received by it, and leads to periodic climatic fluctuations over millennial to million-year timescales. This in turn directly or indirectly influences the Earth's surface system, and leaves its traces in sediments. Milankovitch cycles incorporate sedimentary environments and tectonic changes within the framework of the astronomical rhythm of the Earth's orbital parameters, particularly in highly continuous lacustrine and marine strata. They can accurately illustrate information on climate change within a given basin on an orbital timescale.

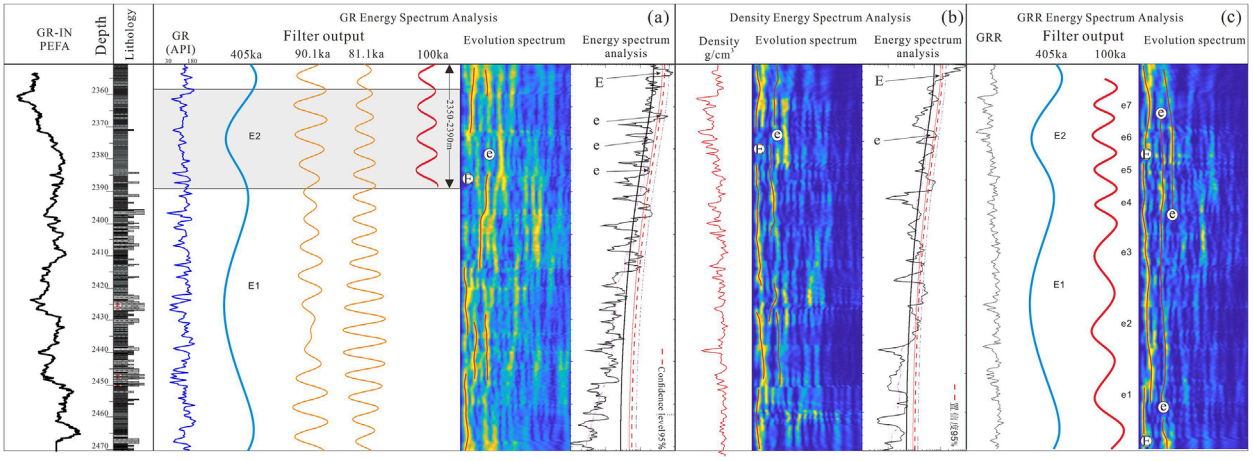

FIGURE 6
Extraction of the astronomical cycles for shallow-lake areas. **(A)** Spectral analysis of the astronomical cycle based on the GR curve. **(B)** Spectral analysis of the astronomical cycle based on the density curve. **(C)** Spectral analysis of the astronomical cycle based on the reconstructed GRR curve. Its characteristics were consistent with those of well SK1 in the deep-lake area.

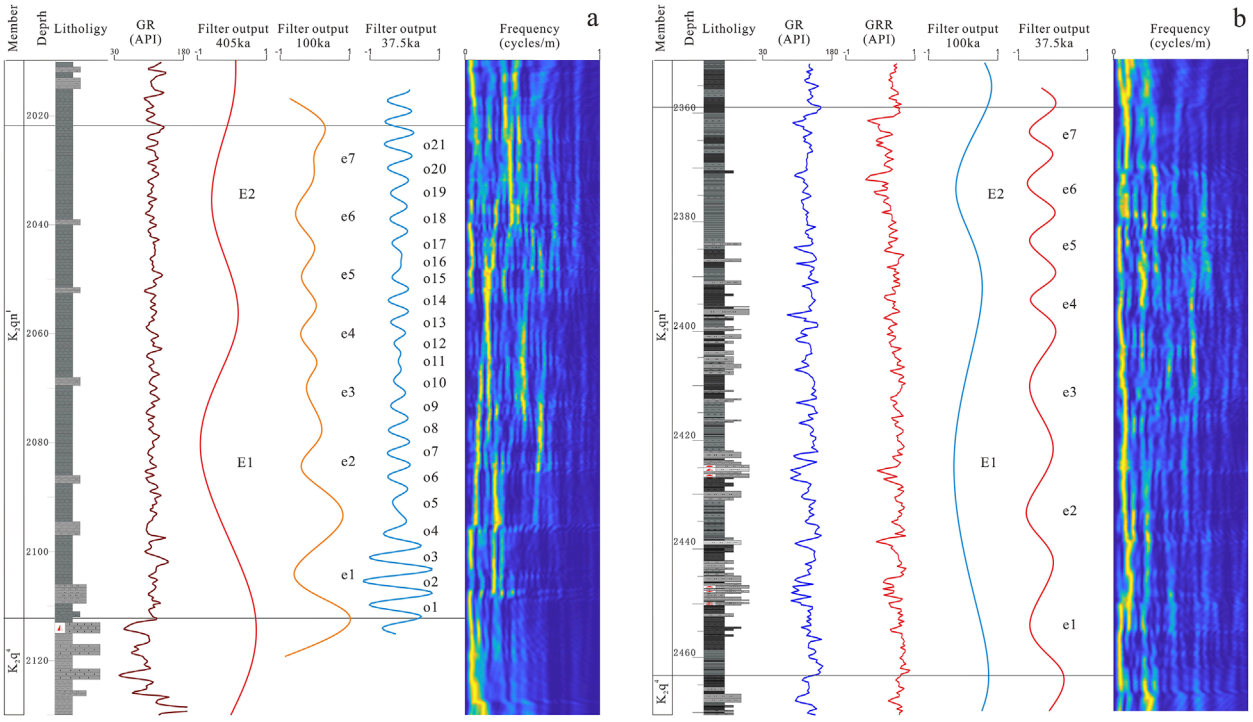

FIGURE 7
Composite stratigraphic column for the extraction of astronomical cycles. **(A)** Well R30: We identified 1.8 long eccentricity cycles, seven short eccentricity cycles, and 21 obliquity cycles in the First Member. Filter passband for 405 ka eccentricity cycles: K_2qn^1—0.0202 ± 0.007 cycles/m. Filter passband for 100 ka eccentricity cycles: K_2qn^1—0.0876 ± 0.021 cycles/m. **(B)** Well Hei 258: The GRR curve identified 1.8 long eccentricity cycles and seven short eccentricity cycles. Filter passband for 405 ka eccentricity cycles: K_2qn^1—0.0217 ± 0.006 cycles/m. Filter passband for 100 ka eccentricity cycles: K_2qn^1—0.087 ± 0.029 cycles/m.

We used sequences of the Milankovitch cycle as a framework, and used it to comprehensively analyze changes in the geochemical parameters based on data on elemental logging. The results showed a significant bipartite sedimentary environment in section K_2qn^1, which was divided at 2396 m (Couch, 1971; Roy and Roser, 2013). The sedimentary noise reflected a continuous rise in the lake level and a gradual deepening of the water body, with a slower change in its depth in the lower part and multiple oscillations in it as well. When the 2396-m boundary was crossed, the rate of rise in the lake level increased significantly and it became

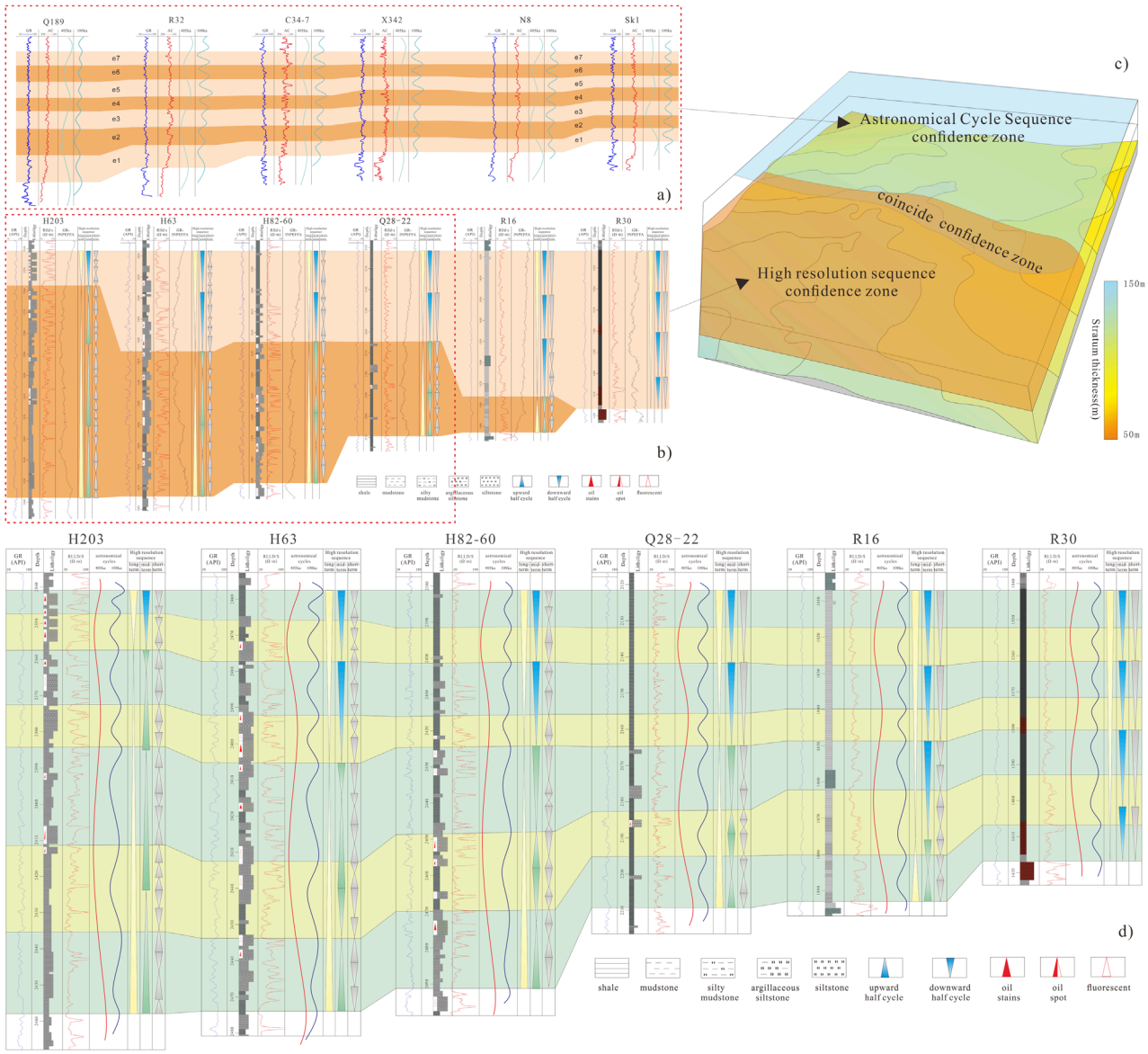

FIGURE 8
Comparison of the range of confidence and results of division between the sequence of astronomical cycles and the high-resolution sequence. **(A)** From well SK1 to well Q189, the stratigraphic framework of astronomical cycles comprised approximately 1.8 complete long eccentricity cycles and seven complete short eccentricity cycles, exhibiting good stability. The confidence interval was primarily located in the southern region. **(B)** From well H203 along the margin of the lake basin to well R30, the resolution of the framework for high-resolution sequential stratigraphy gradually decreased, with poor precision in areas around wells R16 and R30, and the confidence interval was situated in the southern region. **(C)** When the distributions of the confidence intervals of the frameworks for high-resolution sequential stratigraphy and the astronomical cycle-based stratigraphy are combined, the overlapping areas form the integrated confidence interval. The high-resolution sequential and astronomical cyclic stratigraphic frameworks can be fused and extended based on the integrated confidence interval. This enables the formation of stratigraphic frameworks at both scales. **(D)** The high-frequency sequential framework of the margin of the lake basin under astronomical constraints.

considerably deeper. The contents of Mg/Ca, Ca/(Ca+Fe), Th/U, and (Al+Fe)/(Ca+Mg) all exhibited similar characteristics. The lower part of the body of water was mainly shallow and semi-deep, with a semi-arid to semi-humid climate, weakly reducing to weakly oxidizing environment, and oscillatory deepening of the body of water accompanied by the periodic input of terrestrial material. The lake was deeper above the boundary, and was dominated by deep-water deposition with a low rate of sedimentation, increased salinity of water, a relatively humid climate, and enhanced conditions for reduction.

4.3 Characteristics of organic matter

Based on the results of the astronomical cycles as well as the sequential stratigraphy of mud-rich and sand-rich areas, we matched the

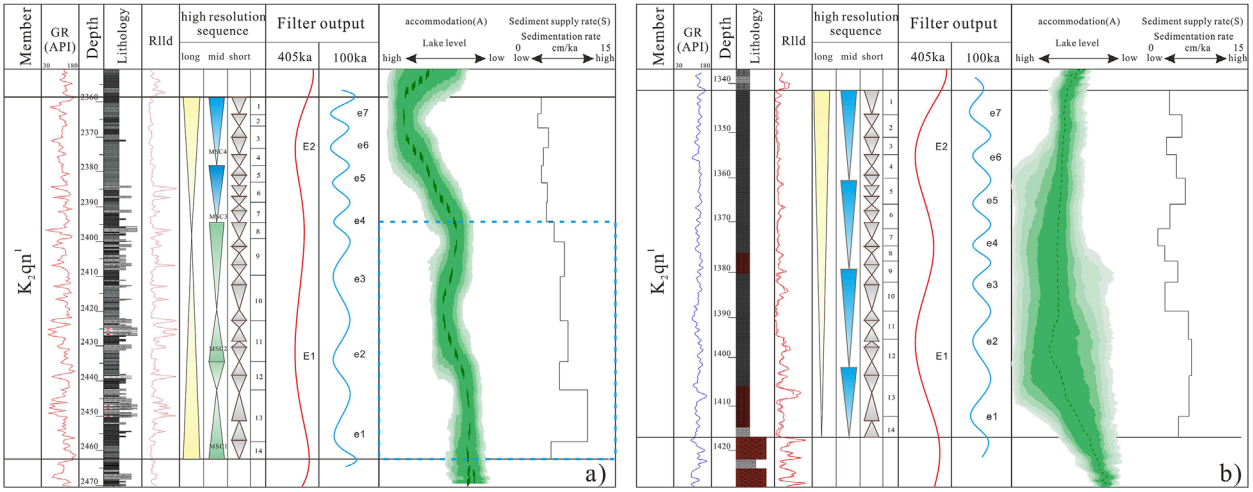

FIGURE 9
Composite columnar sections at the tectonic timescale. **(A)** Well H258 in the sand-rich region. **(B)** Well R30 in the mud-rich region. Curves of the depth of the lake obtained by the DYNOT model indicate an increase in its depth from bottom to top. Correspondingly, the curves of the rate of sedimentation suggest a decreasing sediment supply from bottom to top. The DYNOT models were estimated by using a running window of 405 ka, while the confidence levels were estimated by using Monte Carlo analysis over 5,000 iterations.

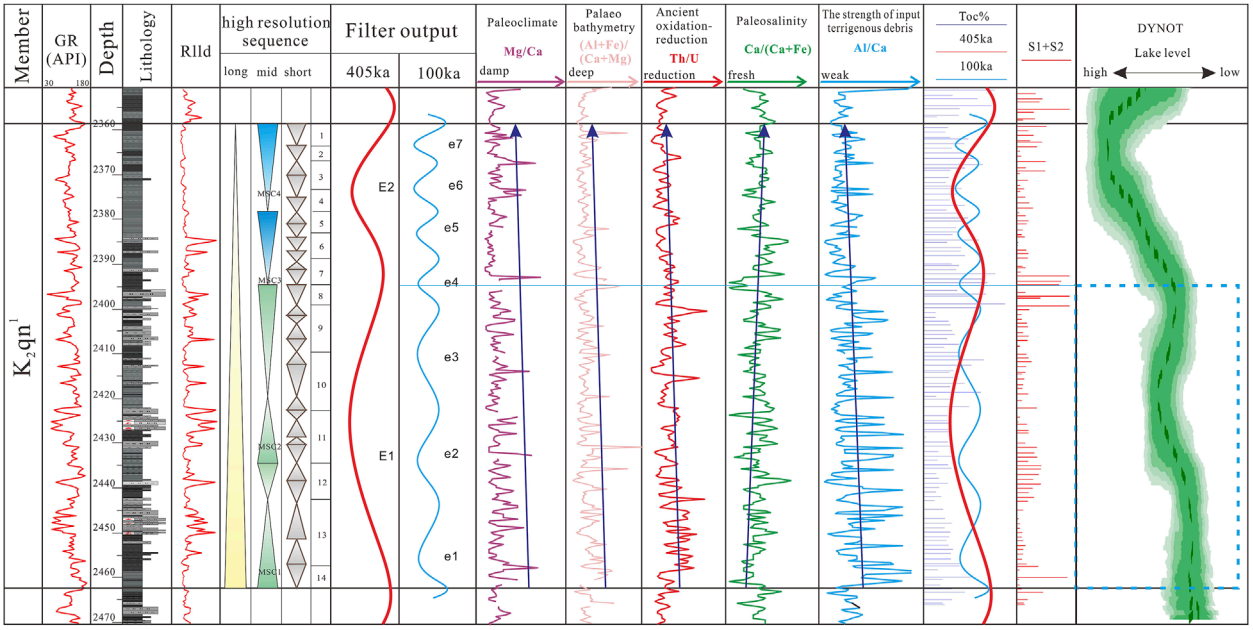

FIGURE 10
Vertical variations in the geochemical parameters, organic matter content, and sedimentary noise for well Hei 258 at the astronomical cycle scale. Its geochemical parameters and sedimentary noise exhibited significant differences above and below the 2396-m boundary. The lower section was characterized by shallow to semi-deep water bodies, a semi-arid to semi-humid climate, and a weakly reductive to weakly oxidizing environment. The depth of water gradually increased with periodic oscillations and the episodic input of terrigenous material. The lake was significantly deeper above the boundary, and was dominated by deep-water deposition with a low rate of sedimentation, increased salinity, a relatively humid climate, and enhanced conditions for reduction. This reflects the clear bipartite nature of the depositional environment of K_2qn^1.

curves of the astronomical cycles with models of the total organic carbon (TOC), geochemical elements, and sedimentary noise to reconstruct environmental changes on an astronomical scale. Consider well HEI258 in the shallow-water area as an example. This stratum contained approximately four long eccentricity cycles and 14 short eccentricity cycles. The latter were well correlated with the characteristics of variations in the TOC. Seven high-TOC zones primarily developed in the First Member (K_2qn^1), which aligns well with the maxima of the 100 ka short eccentricity cycles. This suggests that the patterns of enrichment of organic matter, whether at the center or the margin of the

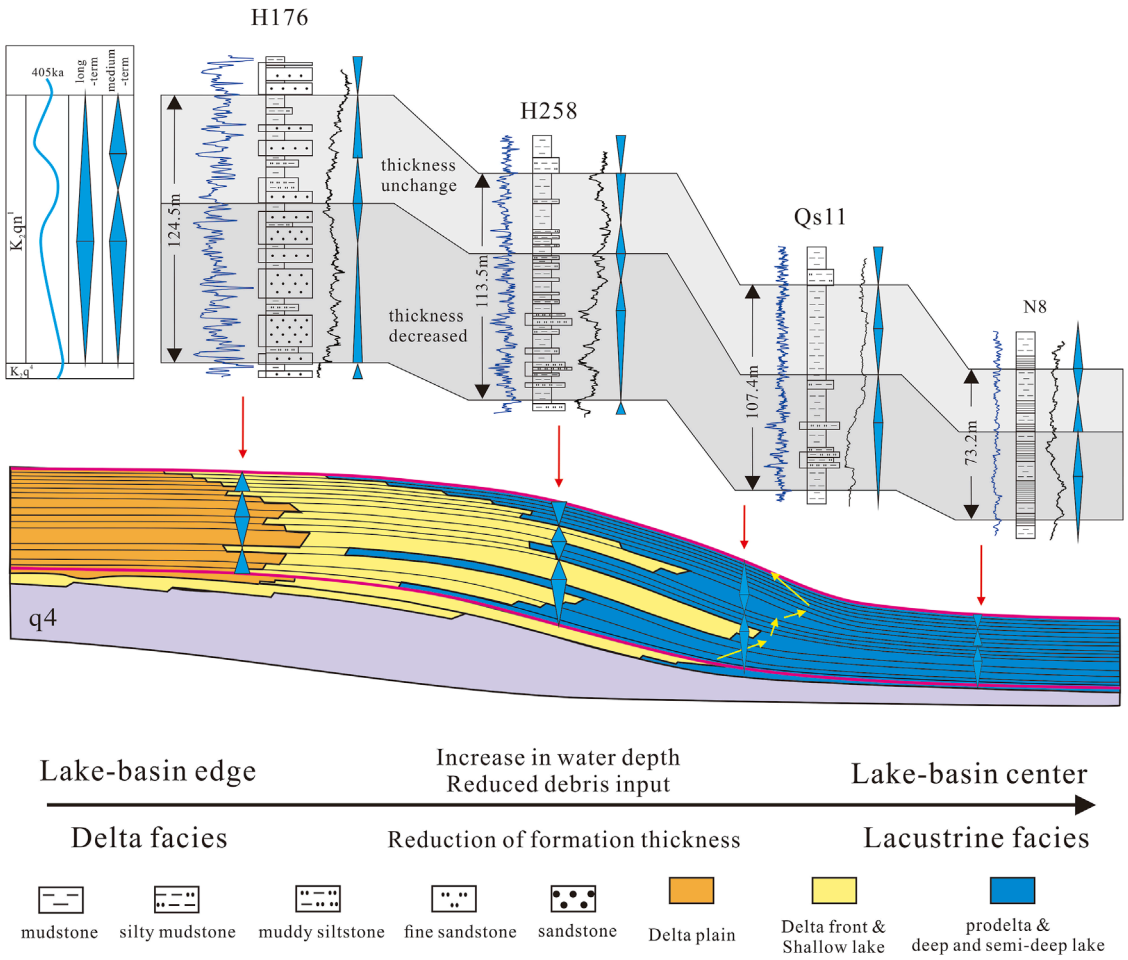

FIGURE 11
Profile of the stratigraphic framework of the deep-water, sand-rich area in the First Member. Wells QS11 and N8 were located along the edge of a shallow lake, where the sand bodies were not developed, and astronomical cycles of 405 ka, 100 ka, and 37.5 ka were observed. Wells Qs11 and H258 were situated along the edge of the delta front near the shallow lake. We unified the frameworks of high-resolution sequential stratigraphy and astronomical cycle stratigraphy by integrating them. The thickness of the upper mud-rich strata remained constant from the sand-rich area to the mud-rich area, while the thickness of the cyclic strata in the lower sand-rich deposits increased due to differences between the rates of sedimentation of sand and mud, which obscured the astronomical signals. This method accurately restored the characteristics of astronomical signals in sand-rich areas.

lake basin, were controlled by the astronomical cycles, although these patterns varied at the vertical level (Figure 10).

The enrichment of organic matter was constrained by primary productivity and subsequent conditions of preservation, which were closely related to the types and patterns of the deposited sediments. We can better reconstruct the original patterns of organic matter accumulation by analyzing sedimentary environments on the same scale as the changes in organic matter enrichment.

5 Discussion

5.1 Models of stratigraphic development and patterns of basin filling

The sedimentation of modern lakes illustrates that the relationship between the supply of sediment and water (mostly climatic), and changes in the potential space to accommodate the sediment (mostly climatic) in each lake controlled its sedimentary characteristics, distribution, and patterns. Our analysis of the types of sediments, their spatial distribution, and evolutionary characteristics based on our model of stratigraphic development confirmed that a delta system for lakes had developed in the southern Songliao Basin, with a gentle slope that was constrained by patterns of "synchronous heterotopy." The supply of the sediment in the model decreased progressively from the land toward the lake basin, the rate of sedimentation decreased, and geomorphologically controlled changes in the space to accommodate the sediment. This led to the general trend of thinning strata toward the center of the lake basin (Figure 11).

The model of stratigraphic development represented the characteristics of sedimentary filling of the basin as well. We used it with the aforementioned characteristics of the tectonic and orbital timescales to conclude that the lake in the study area had undergone two main processes of evolution: an early

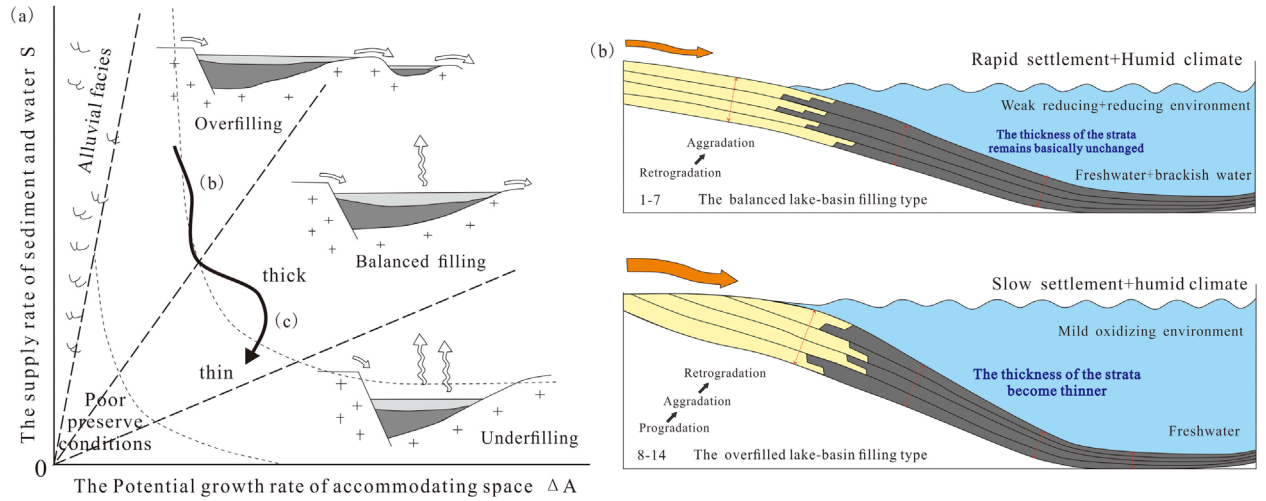

FIGURE 12
Patterns of stratigraphic stacking and sedimentary models from the margin of the basin to its center in the Daqingzi well. **(A)** Patterns of stratigraphic stacking (Carroll and Bohacs, 1999). **(B)** Sedimentary models. A lacustrine delta system developed in the study area that was constrained by a pattern of synchronous heterotopy under a gentle slope. The stratigraphic model was influenced by changes in the space to accommodate the sediment, resulting in progressively thinner strata from the land toward the lake basin. Based on its patterns of stratigraphic stacking, the model can be divided into a lower/shallow-water "overfilled" sedimentary model and an upper/deep-water "balanced filling" sedimentary model. The rates of supply of the sediment and water consistently exceeded the potential space to accommodate them in the "overfilled" sedimentary model. The periodicity (more oscillatory) and progradation of the strata were mainly controlled by the periodic supply of terrigenous clastics. By contrast, the "balanced filling" model featured rates of supply of the sediment and water that were roughly balanced over the span of development of the sequence. The strata exhibited aggradational–retrogradational characteristics, with a periodicity that was consistent with astronomically driven features.

pattern of excessive basin filling followed by a later, more "balanced filling" pattern.

"Overfilled" sedimentary model: There was an abundant supply of sediment in this model, which led to the development of distributary channels in shallow-water deltas. The large influx of terrigenous clastics led to the formation of progradational stratigraphic features (Figure 12). Internal bioclastic material mainly originated from terrestrial input, while other bodies of freshwater carbonates had not developed. They occur when the rates of supply of the sediment and water consistently exceed the potential space to accommodate them. Climatically driven fluctuations in the lake level were minimal, and the periodic increase in terrigenous clastic input owing to the humid climate controlled the oscillatory pattern of sedimentation (Figure 13).

"Balanced filling" sedimentary model: The supply of the sediment was lower in this model, resulting in a deeper lake in which the terrigenous clastic input was less influential, and the stratigraphy exhibited aggradational–retrogradational characteristics (Figure 12). Sedimentation was primarily influenced by fluctuations in the groundwater level due to the chemistry of the water, its temperature, and chemical stratification, and led to the local formation of interbed clastics and carbonates. This occurs when the rates of supply of the sediment and water are balanced with the space to accommodate them over the span of development of the sequence. The inflow of water was sufficient to periodically fill the space, but was not always in equilibrium with it. Hence, astronomically driven characteristics were more pronounced, and climatically driven fluctuations in the lake level led to common periodic sedimentary features in the model (Figure 13).

5.2 Organic matter enrichment under astronomical cycle

The cyclicity of fine-grained lacustrine sedimentary environments and the parameters of the organic matter revealed stratigraphic cyclicity, with a high correlation between the distribution of shale lithofacies and cycles of organic matter enrichment. The average TOC and the highest S1+S2 values of the mudstone layers were always high at the transgressive–regressive positions of transition within the stratigraphic cycles, corresponding to high values of short eccentricity cycles within the astronomical cycles. These were the most favorable facies for the exploration of shale oil. It is evident from the above that organic matter, whether at the edge or the center of the basin, was periodically enriched with a 100 ka limit. This periodicity fitted well at the center of the lake basin but exhibited a lag, with the high-TOC zones vertically positioned in the latter half of the 100 ka (short eccentricity) maximum.

Figures 9, 10 show the clear bipartite nature of the K_2qn^1 in the study area. The rates of supply of the sediment and water, and the rate of increase in the space to accommodate the sediment were roughly balanced over the span of sequential development in the upper part of the deep-water area, exhibiting features that were highly driven by the astronomical cycles. This model of the "balanced filling" of the lake basins was the best combination for the production, preservation, and dilution of organic matter in the basin. The periodic stratification induced by astronomically driven climatic changes provided favorable conditions for its periodic deposition and preservation. OM enrichment was most likely to occur at the transition from a fall in the base level to a rise in it, i.e., at the

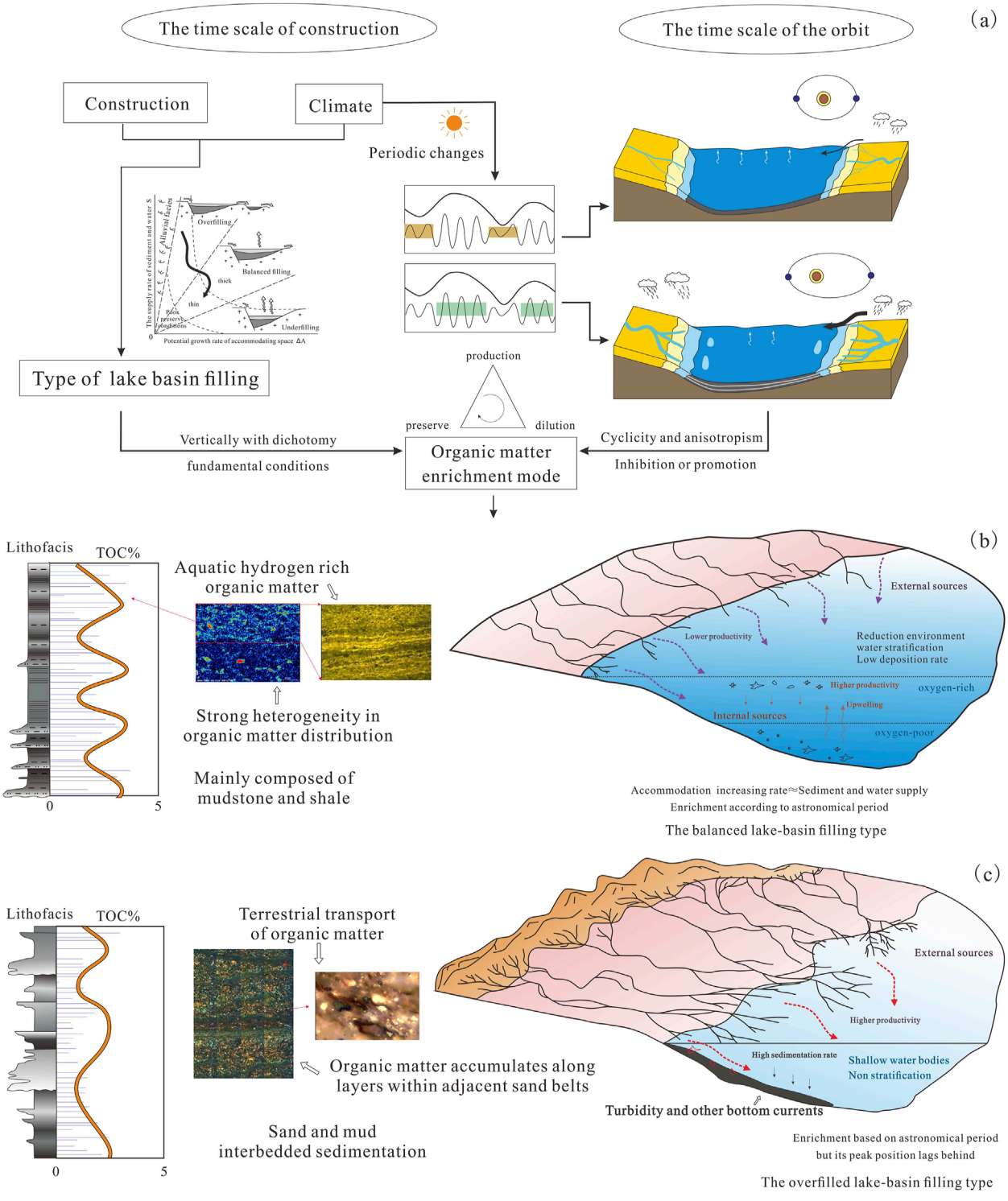

FIGURE 13
Models of the differential enrichment of organic matter from the margin of the lake basin to its center in the Daqingzi well area. The two models differed in the sources of organic matter, mechanisms of its enrichment, and conditions of water during deposition, resulting in different characteristics of enrichment at the astronomical scale. **(A)** The bipartite pattern of filling of the basin arose from varying rates of sediment supply and the space to accommodate it at the tectonic scale. Moreover, the distinct climatic characteristics at the maximum eccentricity at the orbital timescale influenced the patterns of organic matter enrichment. **(B)** The "balanced filling" model of organic matter enrichment of the lake basin in the deep part of the lake shows that the organic matter originated from both within and outside the basin, and exhibited strong heterogeneity. The zones of high enrichment in organic matter aligned with the maxima of short eccentricity. **(C)** The "overfilled" model of organic matter enrichment in the lake basin in the shallow-water area of the lake shows that the organic matter mainly originated from terrestrial plant debris outside the basin. The layers in the siltstone bands featured abundant organic matter, with the zones of high enrichment slightly lagging behind the maxima of short eccentricity.

maximum short eccentricity, matching the 97 ka cycle of deposition of organic matter.

By contrast, the peaks of organic matter along the edges of the sand-rich basin did not strictly correspond to the 100 ka short eccentricity cycles, and exhibited a lag. The model of "overfilled lake basins" featured sound aquatic production and abundant input from terrestrial plants. The main challenges to the concentration of organic matter were its preservation and dilution. The control of density stratification by solutes was unlikely to develop under continuously open hydrological conditions, and required the temperature-influenced stratification of water for the effective preservation of organic matter. Dilution was common owing to the strong riverine influence, and led to a lagged enrichment of the organic matter above the flooding surface, and in the latter part of the maximum of short eccentricity. Moreover, the curves of sedimentary noise reflected an overall transgressive trend in the K_2qn^1. The top of the sand-rich area also began to exhibit the "balanced filling" patterns of organic matter enrichment owing to increased lake depth and reduced terrigenous clastic energy.

6 Conclusion

In this study, we combined the results of astronomical cycle-based and high-resolution stratigraphic delineation to construct a stratigraphic framework of fine-grained, high-frequency sedimentary sequences in a lake, as constrained by the astronomical cycle in the mud-rich zone at the center of the basin and the sand-rich zone along its edge. Our analyses of the sedimentary environment and noise, recovery of the lacustrine level, and geochemical parameters confirmed that the pattern of stratigraphic development of the lake delta system in the study area was constrained according to the model of the "contemporaneous heterogeneous phase," with a gradual decrease in the rate and supply of sediment to the lake basin, a significant change in the geomorphologically controlled space to accommodate it, and the gradual thinning of the stratigraphic layers. This pattern of stratigraphic development controlled the patterns of deposition and distribution of shale that was rich in organic matter.

The cyclic nature of the fine-grained sedimentation of the lake basin revealed the hierarchical nature of the sequence, and the sedimentary strata in the First Member were clearly dichotomous. The features of the lower, early strata suggest that the depositional environment was a low-salinity, weakly oxidized one with relatively shallow water, a strong input of terrestrial debris, and rapid vertical changes in the geochemical parameters. This suggests that the environment fluctuated considerably at this time. By contrast, the water body was significantly deeper, the salinity slightly higher, the reductive nature of the environment was enhanced, the climate shifted from semi-humid to warm and humid, and the input of terrestrial detritus was significantly reduced during the period of deposition of the upper, late sedimentary strata. The difference between the space to accommodate the sediment and the input of terrestrial detritus formed the distinct depositional patterns of the First Member, i.e., the "overfilled" depositional pattern in the lower part of the formation and the "equilibrium" pattern of deposition.

The pattern of fine-grained sedimentation had an important influence on organic matter enrichment, the balanced lake-basin filling type organic matter enrichment pattern in the deep-water area of the lake, at this time, the source of organic matter inside and outside of the basin, non-homogeneous and strong, organic matter enrichment of the high value of the area and the location of the maximum value of the short eccentricity is the same. The organic matter mainly originated from terrestrial plant debris outside the basin, according to the model of the "overfilled" pattern of organic matter enrichment of the lake basin. It filled the silt zone along the layer, the OM content of which slightly lagged behind the position of the extremum of the short eccentricity.

Data availability statement

The original contributions presented in the study are included in the article/supplementary material, further inquiries can be directed to the corresponding author.

Author contributions

XW: Writing–original draft, Writing–review and editing. YS: Writing–review and editing. LY: Writing–review and editing. ZT: Writing–review and editing. BY: Writing–review and editing. RL: Writing–original draft, Writing–review and editing.

Funding

The author(s) declare that financial support was received for the research, authorship, and/or publication of this article. This research was funded by the Heilongjiang Provincial Natural Science Foundation of China (No. ZD2023D002) and Project of Sanya Yazhou Bay Science and Technology City (No. SCKJ-JYRC-2022-09).

Conflict of interest

Authors LY and ZT were employed by PetroChina Jilin Oilfield Company.

The remaining authors declare that the research was conducted in the absence of any commercial or financial relationships that could be construed as a potential conflict of interest.

Publisher's note

References

Bechtel, A., Jia, J. L., Strobl, S. A. I., Sachsenhofer, R. F., Püttmann, W., Gratzer, R., et al. (2012). Palaeo-environmental conditions during deposition of the Upper Cretaceous oil shale sequences in the Songliao Basin (NE China): implications from geochemical analysis. *Org. Geochem.* 46, 76–95. doi:10.1016/j.orggeochem.2012.02.003

Boulila, S., Dupont-Nivet, G., Galbrun, B., Bauer, H., and Chteauneuf, J. J. (2021). *Age and driving mechanisms of the Eocene-Oligocene Transition from astronomical tuning of a lacustrine record (Rennes Basin, France)*. Copernicus GmbH. doi:10.5194/cp-2021-46

Calvert, S. E., and Pedersen, T. F. (1993). Geochemistry of recent oxic and anoxic marine sediments: implications for the geological record. *Mar. Geol.* 113 (1-2), 67–88. doi:10.1016/0025-3227(93)90150-t

Cao, H. S., Kaufman, A. J., Shan, X. L., Cui, H., and Zhang, G. J. (2016). Sulfur isotope constraints on marine transgression in the lacustrine Upper Cretaceous Songliao Basin, northeastern China. *Palaeogeogr. Palaeoclimatol. Palaeoecol.* 451, 152–163. doi:10.1016/j.palaeo.2016.02.041

Carroll, A. R., and Bohacs, K. M. (1999). Stratigraphic classification of ancient lakes: balancing tectonic and climatic controls. *Geology* 27, 99–102. doi:10.1130/0091-7613(1999)027<0099:scoalb>2.3.co;2

Cheng, X. L., Zhou, X. J., and Guo, J. H. (2003). Study on the sequence stratigraphy of T-R cycles and subtle oil pools in the Dongpu Depression. *Petroleum Geol. and Exp.* (S1), 548–552+556.

Cohen, A. S. (2003). *Paleolimnology: the history and evolution of lake systems*. Oxford University Press.

Couch, E. L. (1971). Calculation of paleosalinities from boron and clay mineral data. *AAPG Bull.* 55 (10), 1829–1837. doi:10.1306/819a3dac-16c5-11d7-8645000102c1865d

Cross, T. A. (1994). High-resolution stratigraphic correlation from the perspective of baselevelcycles and sediment accommodation, in *Proceeding of northwestern European sequence stratigraphy congress*, 105–123.

Demaison, G. J., and Moore, G. T. (1980). Anoxic environments and oil source bed genesis. *Org. Geochem.* 64. doi:10.1306/2f91945e-16ce-11d7-8645000102c1865d

Dong, M. Z., Gong, H. J., Sang, Q., Zhao, X. Y., and Zhu, C. F. (2022). Review of CO2-kerogen interaction and its effects on enhanced oil recovery and carbon sequestration in shale oil reservoirs. *Resour. Chem. Mater.* 1 (1), 93–113. ISSN 2772-4433. doi:10.1016/j.recm.2022.01.006

Du, X. B., Liu, H., Liu, H. M., Lu, Y. C., Wang, Y., Hao, X. F., et al. (2016). Methods of sequence stratigraphy in the fine-grained sediments: a case from the upper fourth sub-member and the lower third sub-member of the shahejie Formation in well fanye 1 of dongying depression. *Bull. Geol. Sci. Technol.* 35 (04), 1–11.

Feng, L. Y., Zhang, J. G., Jiang, Z. X., Li, C. S., and Bai, Y. F. (2023). High-precision sedimentary cycle framework and organic matter enrichment response of Qinghsankou Formation in Songliao Basin. *Acta Pet. Sin.* 44 (02), 299–311. doi:10.7623/syxb202302006

Feng, Z. Q., Jia, C. Z., Xie, X. N., Zhang, S., Feng, Z. H., and Cross, T. A. (2010). Tectonostratigraphic units and stratigraphic sequences of the nonmarine Songliao basin, northeast China. *Basin Res.* 22 (1), 79–95. doi:10.1111/j.1365-2117.2009.00445.x

Hesselbo, S. P. (1996). "Spectral gamma-ray logs in relation to clay mineralogy and sequence stratigraphy," in *Cenozoic of the Atlantic margin*. offshore New Jersey.

Hilgen, F. J., Hinnov, L. A., Abdul Aziz, H., Abels, H. A., Batenburg, S., Bosmans, J. H. C., et al. (2015). Stratigraphic continuity and fragmentary sedimentation: the success of cyclostratigraphy as part of integrated stratigraphy. *.Geol. Soc.* 404, 157–197. doi:10.1144/sp404.12

Houston, J. (2004). High-resolution sequence stratigraphy as a tool in hydrogeological exploration in the Atacam a Desert. *Q. J. Eng. Geol. Hydrogeology* 37 (1), 7–17. doi:10.1144/1470-9236/03-013

Huang, H., Gao, Y., Ma, C., Jones, M. M., Wang, C., Ibarra, D. E., et al. (2023). Organic carbon burial is paced by a~173-ka obliquity cycle in the middle to high latitudes. *Sci. Adv.* 7 (28), eabf9489. [2023-07-05]. doi:10.1126/sciadv.abf9489

Jia, J. L., Bechtel, A., Liu, Z. J., Strobl, S. A. I., Sun, P. C., and Sachsenhofer, R. F. (2013b). Oil shale Formation in the upper cretaceous Nenjiang Formation of the Songliao Basin (NE China): implications from organic and inorganic geochemical analyses. *Int. J. Coal Geol.* 113 (Complete), 11–26. doi:10.1016/j.coal.2013.03.004

Jia, J. L., Liu, Z. J., Bechtel, A., Susanne, A. I. S., and Sun, P. (2013a). Tectonic and climate control of oil shale deposition in the upper cretaceous Qingshankou Formation (Songliao Basin, NE China). *Int. J. Earth Sci.* 102 (6), 1717–1734. doi:10.1007/s00531-013-0903-7

Kemp, D. B. (2011). Shallow-water records of astronomical forcing and the eccentricity paradox. *Geology* 39 (5), 491–494. doi:10.1130/g31878.1

Laskar, J., Fienga, A., Gastineau, M., and Manche, H. (2011). La2010: a new orbital solution for the long-term motion of the earth. *Astronomy and Astrophysics* 532 (2), A89–A785. doi:10.1051/0004-6361/201116836

Li, M. S., Hinnov, L. A., Huang, C. J., and Ogg, J. G. (2018). Sedimentary noise and sea levels linked to land-ocean water exchange and obliquity forcing. *Nat. Commun.* 9 (1), 1004. doi:10.1038/s41467-018-03454-y

Li, M. S., Huang, C. J., Ogg, J., Zhang, Y., Hinnov, L. A., Wu, H. C., et al. (2019). Paleoclimate proxies for cyclostratigraphy: comparative analysis using a Lower Triassic marine section in South China. *Earth-Science Rev.* 189, 125–146. doi:10.1016/j.earscirev.2019.01.011

Li, M. S., Ogg, J., Zhang, Y., Huang, C. J., Hinnov, L., Chen, Z. Q., et al. (2016). Astronomical tuning of the end-permian extinction and the early triassic epoch of south China and Germany. *Earth and Planet. Sci. Lett.* 441, 10–25. doi:10.1016/j.epsl.2016.02.017

Li, Q. Z., Chen, J. L., Zou, H., Wang, C. S., Meng, Q. A., Liu, H. L., et al. (2020). Mesozoic–cenozoic tectonic evolution and dynamics of the Songliao Basin, NE asia: implications for the closure of the paleo-asian ocean and mongol-okhotsk ocean and subduction of the paleo-pacific ocean. *Earth-Science Rev.* 218, 103471. doi:10.1016/j.earscirev.2020.103471

Liu, B., Sun, J. H., Zhang, Y. Q., He, J. L., Fu, X. F., Yang, L., et al. (2021). Reservoir space and enrichment model of shale oil in the first member of Cretaceous Qingshankou Formation in the Changling Sag, southern Songliao Basin, NE China. *Petroleum Explor. Dev.* 48 (3), 608–624. doi:10.1016/s1876-3804(21)60049-6

Liu, B., Wang, H., Fu, X., Bai, Y., Bai, L. H., Jia, M. C., et al. (2019). Lithofacies and depositional setting of a highly prospective lacustrine shale oil succession from the Upper Cretaceous Qingshankou Formation in the Gulong sag, northern Songliao Basin, northeast China. *AAPG Bull.* (2), 103. doi:10.1306/08031817416

Liu, Q. Y., Shi, J. Y., Jin, Z. J., Liu, Q., Huang, Z. K., and Zhang, R. (2019). Quantitative classification of high-frequency sequences in fine-grained lacustrine sedimentary rocks based on Milankovitch theory. *Oil&Gas Geol.* 40 (06), 1205–1214.

Liu, R. H., Sun, Y., Wang, X. R., Yan, B. Q., Yu, L. M., and Li, Z. (2023). Production capacity variations of horizontal wells in tight reservoirs controlled by the structural characteristics of composite sand bodies: fuyu Formation in the qian'an area of the Songliao Basin as an example. *Processes* 11, 1824. doi:10.3390/pr11061824

Liu, W., Liu, M., Yang, T., Liu, X., Them, T. R., Wang, K., et al. (2022). Organic matter accumulations in the santonian-campanian (upper cretaceous) lacustrine Nenjiang shale (K2n) in the Songliao Basin, NE China: terrestrial responses to OAE3? *Int. J. Coal Geol.* 260, 104069. doi:10.1016/j.coal.2022.104069

Ma, Y., Sun, Y. H., Feng, J. L., Liu, Y., and Yin, C. H. (2022). Study on differential enrichment mechanisms of organic matter in a typical lithofacies fine-grained sag, Songliao Basin. *Acta Sedimentol. Sin.*, 1–21. [2024-09-13]. doi:10.14027/j.issn.1000-0550.2023.037

Milankovitch, M. (1941). *Kanon der Erdbestrahlung und seine Anwendung auf das Eiszeitenproblem*. Academic Serbe, 133.

Olga, O., Grzegorz, M., Marek, S., Filipek, A., Więcław, D., Perotta, I. D., et al. (2023). Spatial distribution of micro- and nanoporosity in Oligocene Menilite and Cretaceous Lgota mudstones (Outer Carpathians): organic porosity development as a key to understanding unconventional hydrocarbon reservoirs. *Mar. Petroleum Geol.* 148 (2023), 106028. ISSN 0264-8172. doi:10.1016/j.marpetgeo.2022.106028

Pan, S. Q., Zou, C. N., Li, Y., Jing, Z. H., Liu, E. T., Yuan, M., et al. (2021). Major biological events and fossil energy formation: on the development of energy science under the earth system framework. *Petroleum Explor. Dev.* 48 (3), 581–594. doi:10.1016/s1876-3804(21)60047-2

Roy, D. K., and Roser, B. P. (2013). Climatic control on the composition of carboniferous–permian gondwana sediments, khalaspir basin, Bangladesh. *Gondwana Res.* 23 (3), 1163–1171. doi:10.1016/j.gr.2012.07.006

Song, Y., Liu, Z., Meng, Q., Xu, J., Sun, P. C., Cheng, L. J., et al. (2016). Multiple controlling factors of the enrichment of organic matter in the upper cretaceous oil shale sequences of the Songliao Basin, NE China: implications from geochemical analyses. *Oil Shale* 33 (2), 142. doi:10.3176/oil.2016.2.04

Sun, S., Liu, H., Cao, Y., Zhang, S., Wang, Y., and Yang, W. (2017). Milankovitch cycle of lacustrine deepwater fine-grained sedimentary rocks and its significance to shale oil: a case study of the upper Es4 member of well NY1 in Dongying sag. *J. China Univ. Min. and Technol.* 46 (04), 846–858. doi:10.13247/j.cnki.jcumt.000638

Sun, Y. (2010). "A study on high-resolution sequence stratigraphy and rule of hydro-carbon accumulations of lithologic reservoirs in meandering river delta ——example of fuyu oil layer in the liangjingdong-mutounan area," in *Northeast petroleum university*.

Tyson, R. V. (2005). The "productivity versus preservation" controversy: cause, flaws, and resolution.

Wang, C. S., Huang, Y. J., and Zhao, X. X. (2009). Unlocking a Cretaceous geologic and geophysical puzzle: scientific drilling of Songliao Basin in northeast China. *Lead. Edge* 28, 340–344. doi:10.1190/1.3104081

Wang, H. R., Guo, Y. J., Huang, Y. M., Yu, C. Q., Huo, Z. P., Li, X. L., et al. (2023d). Morphologies, patterns, and filling architectures at the confluence zones of the cretaceous shallow-water delta in the Songliao Basin, NE China. *J. Asian Earth Sci.* 254, 105758–109120. doi:10.1016/j.jseaes.2023.105758

Wang, K., Ma, L., and Taylor, K. G. (2022a). Nanoscale geochemical heterogeneity of organic matter in thermally-mature shales: an AFM-IR study. *Fuel* 310, 122278. doi:10.1016/j.fuel.2021.122278

Wang, L., Zhang, R., Hua, G. L., and Zhang, L. (2018). On stratigraphy from spatial and temporal perspectives: review and interpretation. *Acta Sedimentol. Sin.* 36 (06), 1059–1074. doi:10.14027/j.issn.1000-0550.2018.091

Wang, M., Chen, H. H., Huang, C. J., Kemp, D. B., Xu, T. W., Zhang, H. G., et al. (2020). Astronomical forcing and sedimentary noise modeling of lake-level changes in the paleogene dongpu depression of north China. *Earth Planet. Sci. Lett.* 535, 116116. doi:10.1016/j.epsl.2020.116116

Wang, M., Zhang, Y. C., Li, J. B., Ma, R., Wang, X., Li, Y., et al. (2023c). Thermal and nonthermal effect of microwave irradiation on the pore microstructure and hydrocarbon generation of organic matter in shale. *Mar. Petroleum Geol.* 150, 106151. doi:10.1016/j.marpetgeo.2023.106151

Wang, P. J., Xie, X. A., Frank, M., Ren, Y. G., Zhu, D. F., and Sun, X. M. (2007). The cretaceous Songliao Basin: volcanogenic succession, sedimentary sequence and tectonic evolution, NE China. *Acta Geol. Sin.* 81, 1002–1011. doi:10.1111/j.1755-6724.2007.tb01022.x

Wang, W. X. (2022b). Study on sandbody distribution in sequence stratigraphic framework of the first member of Qingshankou Formation in Hei258 block, Songliao Basin. *Northeast Pet. Univ.*

Wang, X. R., Sun, Y., Liu, R. H., and Li, Z. (2023a). Research progress into fine-grained sedimentary rock characteristics and formation in a continental lake basin. *Acta Sedimentol. Sin.* 41 (2), 349–377. doi:10.14027/j.issn.1000-0550.2021.117

Wang, Y. C., Li, P. P., Feng, Z. H., Shao, H. M., Jia, Z. W., Xia, Y. Q., et al. (2023b). Geochemical characteristics of shales from the first member of Qingshankou Formation in Gulong Sag, Songliao Basin, China: implication for mechanism of organic matter enrichment. *Mar. Petroleum Geol.* 150, 106142. ISSN 0264-8172. doi:10.1016/j.marpetgeo.2023.106142

Wu, H. C., Hinnov, L. A., Zhang, S. H., Jiang, G. Q., Yang, T. S., Li, H. Y., et al. (2022). Continental geological evidence for solar system chaotic behavior in the late cretaceous. *GSA Bull.* 135 (3-4), 712–724. doi:10.1130/b36340.1

Wu, H. C., Zhang, S. H., Hinnov, L. A., Jiang, G. Q., Yang, T. S., Li, H. Y., et al. (2014). Cyclostratigraphy and orbital tuning of the terrestrial upper santonian–lower danian in Songliao Basin, northeastern China. *Earth Planet. Sci. Lett.* 407 (407), 82–95. doi:10.1016/j.epsl.2014.09.038

Wu, H. C., Zhang, S. H., Jiang, G. Q., Hinnov, L. A., Yang, T. S., Li, H. Y., et al. (2013). Astrochronology of the early turonian–early campanian terrestrial succession in the Songliao Basin, northeastern China and its implication for long-period behavior of the solar system. *Palaeogeogr. Palaeoclimatol. Palaeoecol.* 385, 55–70. doi:10.1016/j.palaeo.2012.09.004

Wu, H. C., Zhang, S. H., Jiang, G. Q., and Huang, Q. H. (2009). The floating astronomical time scale for the terrestrial Late Cretaceous Qingshankou Formation from the Songliao Basin of Northeast China and its stratigraphic and paleoclimate implications. *Earth Planet. Sci. Lett.* 278 (3-4), 308–323. doi:10.1016/j.epsl.2008.12.016

Xu, J. J., Liu, Z. J., Bechtel, A., Meng, Q. T., Sun, P. C., Jia, J. L., et al. (2015). Basin evolution and oil shale deposition during Upper Cretaceous in the Songliao Basin (NE China): implications from sequence stratigraphy and geochemistry. *Int. J. Coal Geol.* 149, 9–23. doi:10.1016/j.coal.2015.07.005

Xu, J. J., Liu, Z. J., Bechtel, A., Sachsenhofer, R. F., Jia, J. L., Meng, Q. T., et al. (2019a). Organic matter accumulation in the upper cretaceous Qingshankou and Nenjiang formations, Songliao Basin (NE China): implications from high-resolution geochemical analysis. *Mar. Petroleum Geol.* 102, 187–201. doi:10.1016/j.marpetgeo.2018.12.037

Xu, K., Chen, H. H., Huang, C. J., Ogg, J. G., Zhu, J. X., Lin, S. Q., et al. (2019b). Astronomical time scale of the Paleogene lacustrine paleoclimate record from the Nanxiang Basin, central China. *Palaeogeogr. Palaeoclimatol. Palaeoecol.* 532, 109253. doi:10.1016/j.palaeo.2019.109253

Yu, F. N., Sun, P. C., Zhao, K. G., Ma, L., and Tian, X. M. (2020). Experimental constraints on the evolution of organic matter in oil shales during heating: implications for enhanced *in situ* oil recovery from oil shales. *Fuel.* 261, 116412–116412.14. doi:10.1016/j.fuel.2019.116412

Zhang, P. L., David, M., Hu, F., Nikolaos, K., Reinhard, S., Liu, Z. J., et al. (2021). Porosity evolution in organic matter-rich shales (Qingshankou Fm.; Songliao Basin, NE China): implications for shale oil retention. *Mar. Petroleum Geol.* 130 (1), 105139. doi:10.1016/j.marpetgeo.2021.105139

Zhang, P. L., Misch, D., Meng, Q. T., Sachsenhofer, R. F., Liu, Z. J., Jia, J. L., et al. (2022). Lateral changes of organic matter preservation in the lacustrine Qingshankou Formation (Cretaceous Songliao Basin, NE China): evidence for basin segmentation. *Int. J. Coal Geol.* 254, 103984. ISSN 0166-5162. doi:10.1016/j.coal.2022.103984

Zhang, P. L., Xu, Y. B., Meng, Q. T., Liu, Z. J., Zhang, J. Q., Shen, L., et al. (2020). Sequence stratigraphy and geochemistry of oil shale deposits in the upper cretaceous Qingshankou Formation of the Songliao Basin, NE China: implications for the geological optimization of *in situ* oil shale conversion processing. *Energies* 13, 2964. doi:10.3390/en13112964

Zhang, R., Jin, Z. J., Liu, Q. Y., Li, P., Huang, Z. K., Shi, J. Y., et al. (2019). Astronomical constraints on deposition of the middle triassic chang 7 lacustrine shales in the ordos basin, Central China. *Palaeogeogr. Palaeoclimatol. Palaeoecol.* 528, 87–98. doi:10.1016/j.palaeo.2019.04.030

Zheng, R. C., Peng, J., and Wu, C. R. (2001). Grade division of base-level cycles of terrigenous basin and its implications. *Acta Sedimentol. Sin.* 19 (02), 7.